ASSESSMENT OF CHLORIDE RESISTANCE AND BINDING MECHANISM OF PORTLAND-LIMESTONE CEMENT (PLC) CONCRETE

Chengkai Wang

A thesis submitted to the University of Ottawa in partial fulfillment
of the requirements for the degree of

MASTER OF APPLIED SCIENCE IN CIVIL ENGINEERING

Under the supervision of Dr. Leandro Sanchez

Department of Civil Engineering
Faculty of Engineering
University of Ottawa

Abstract

Concrete production is responsible for approximately 8% of global CO_2 emissions, primarily due to the high clinker content and energy demands associated with Portland cement (PC) manufacturing. In response to growing environmental concerns, Portland-limestone cement (PLC), which partially replaces clinker with interground limestone, and the use of supplementary cementitious materials (SCMs) such as fly ash and slag have been widely promoted as low-carbon alternatives. However, the durability performance of high-limestone PLC systems remains a topic of concern, particularly in terms of chloride ingress resistance and associated binding behavior. This study investigates the chloride resistance and chloride binding capacity of fifteen PLC concrete mixtures, incorporating varying limestone replacement levels and SCM types, under a water-to-powder ratio (W/P) of 0.4. A combination of bulk diffusion testing and acceleration tests was employed. Chloride binding was assessed using both acid-soluble and water-soluble extractions to quantify total and free chloride contents. The results show that SCMs significantly enhance chloride resistance. A strong correlation was observed between electrical resistivity and the apparent diffusion coefficient (Da), emphasizing the role of pore structure in chloride resistance under PLC systems. Moreover, the Langmuir isotherms provided the best fit for chloride binding behavior across all pure PLC mixtures, and analysis revealed that the Al_2O_3/SO_3 ratio, rather than the Al_2O_3 content, is a more reliable indicator of chloride binding capacity. While fly ash contributed to enhanced chloride binding, the effect of slag was less dependent on the limestone content due to its different chemical binding mechanisms. These findings underscore the need for a high quality control of cement manufacturing along with optimized concrete mix proportioning to ensure the reliable performance of high-limestone, low-carbon PLC mixtures in chloride-exposed environments.

Keywords: Portland-limestone cement (PLC), chloride resistance, chloride binding, supplementary cementitious materials (SCMs), fly ash, slag.

Acknowledgements

First of all, I want to give my best appreciation to my supervisor, Prof. Leandro Sanchez. From our first time seeing each other in your graduate class until today, I could see my improvement under your detailed guidance. Professor, thank you again for providing me with this stage to let me know how nice the research is, and it is my fortune to meet you, nothing is better than you being my supervisor.

I would also like to thank you to everyone in our μstructure group. When I first came to our group, I was like a "blank paper," and I had no idea how to work and schedule my project, with everyone's help, I became less stressed and familiar with each test related to my project. Everyone's motivation makes this a great team and, to me, a family!

I would like to express my sincere gratitude for all of the help I gained in laboratory work from the technical officers, Dr. Gamal Elnabelsya, Dr. Muslim Majeed in the Structural and Material lab and Tram Nguyen in the Environmental Engineering lab. Thanks again for all of your help.

Finally, I want to thank my parents. Without your endless support, I cannot make it happen. I especially want to tell my dad: you are the real "MVP" in my life! I remember our every talk when I came to Canada, I totally know how hard you worked to support my dream. As you said: "Kai, the meaningful life is waiting for you; keep going, and I am always your back." Dad, I love you!

Table of Contents

List of Figures

List of Tables

List of Abbreviations

PLC	Portland-limestone cement
PC	Portland cement
SCMs	Supplementary cementitious materials
C-A-S-H	Calcium aluminosilicate hydrate
AFm	Monosulfate
AFt	Ettringite
Mc	Monocarboaluminate
$Ca(OH)_2$	Calcium hydroxide
NaCl	Sodium chloride
$AgNO_3$	Silver nitrate
NaOH	Sodium hydroxide
Al_2O_3	Aluminum oxide
SO_3	Sulfur trioxide
RCPT	Rapid chloride permeability test
ER	Electrical resistivity
Bulk ER	Bulk electrical resistivity
Surface ER	Surface electrical resistivity
XRD	X-ray diffraction
TGA	Thermogravimetric analysis
XRF	X-ray fluorescence
Da	Apparent diffusion coefficient
W/P	Water-to-powder ratio

Chapter 1

Introduction

Concrete is the second most consumed material globally, following only water, and is responsible for approximately 8% of global CO_2 emissions. The primary contributor to this environmental burden is Portland cement (PC), due to its carbon- and energy-intensive manufacturing process [1], [2]. In response to growing climate concerns and national carbon reduction targets, such as Canada's Net-Zero Emissions initiative, which aims for a 40% reduction by 2030 and net-zero by 2050 [3], there is an increasing interest in the development of low-carbon cementitious systems. Two widely studied strategies for reducing clinker content in concrete include the use of Portland-limestone cement (PLC), which incorporates interground limestone to partially replace clinker [4], as shown in Figure 1.1, and the blending of supplementary cementitious materials (SCMs), such as fly ash and slag, which are industrial by-products [5]. Both approaches contribute to a reduction in CO2 emissions while preserving the mechanical and durability properties of concrete.

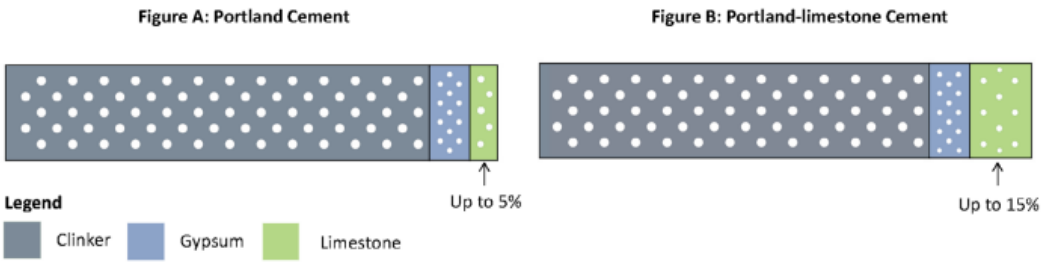

Figure 1.1 Particle Composition differences between PC and PLC [4].

Chloride-induced corrosion remains one of the most severe degradation mechanisms in reinforced concrete infrastructure. Chloride ions from de-icing salts or marine exposure can penetrate concrete, reach the steel reinforcement, and initiate corrosion [6,7]. Chloride resistance is controlled by two primary mechanisms: chloride binding and the pore structure of the concrete matrix, which is illustrated in Figure 1.2. Chloride ions may chemically bind with AFm phases to form Friedel's

salt or physically adsorb onto C-A-S-H gel within the cementitious matrix [7-9]. Effective chloride binding and refinement of concrete pore structure delay corrosion initiation.

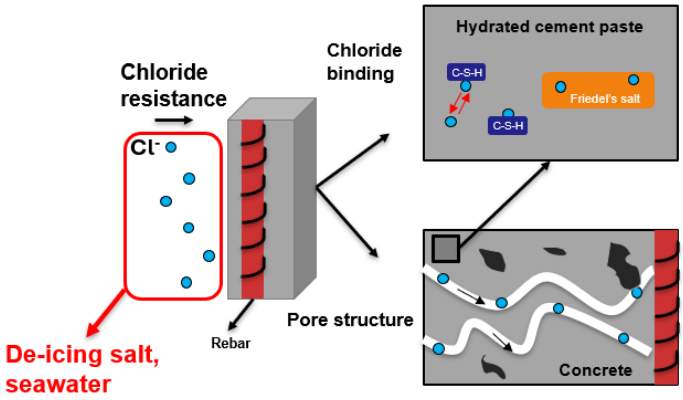

Figure 1.2 Schematic of chloride resistance.

According to CSA A3000-23 [10], the maximum allowable limestone content in PLC is 15%. Extensive research has shown that PLC with this level of replacement performs comparably to PC in terms of strength, workability, and durability, including chloride resistance [11,12]. However, in pursuit of further decarbonization, higher limestone replacement levels (i.e., over 15%) are increasingly being considered. While these mixes offer greater sustainability potential, they also raise concerns regarding long-term durability, particularly in chloride resistance performance.

1.1 Research objectives and scope of the work

While chloride resistance in PC systems has been extensively studied, there remains a knowledge gap regarding PLC systems, particularly those with higher limestone content and SCM incorporation. The present study addresses this gap by evaluating the chloride resistance and associated binding capacity of PLC concretes incorporating varying limestone replacement levels and SCM types. Multiple test methods, including bulk diffusion and acceleration tests, are used to provide a comprehensive understanding of performance in low-carbon concrete systems. Through this comprehensive approach, the study also seeks to provide new insights into the performance of high-limestone PLC systems and explore the influence of cement chemistry on chloride resistance.

The findings aim to support the broader implementation of sustainable, low-carbon concrete technologies without compromising long-term performance.

1.2 Thesis organization

This thesis is structured into five chapters, each addressing a key component of the research. Chapter 1 (Introduction) presents an overview of Portland-limestone cement (PLC) and the impact of chloride ingress on concrete durability. It outlines the motivation behind exploring alternative cement systems with reduced carbon emissions and enhanced long-term performance. Chapter 2 (Background) provides a detailed literature review on the use of PLC and supplementary cementitious materials (SCMs) as strategies to reduce CO_2 emissions. It further discusses the influence of these materials on chloride resistance, followed by a review of current testing methods for evaluating chloride binding and chloride resistance in concrete. The chapter concludes by identifying key research gaps and outlining the challenges associated with implementing high-limestone PLC in durability-critical applications. Chapters 3 and 4 are presented in the form of two research papers. Paper 1 (Chapter 3) investigates the overall chloride resistance of PLC concretes using a range of experimental methods, including bulk diffusion, electrical resistivity (i.e., bulk ER and surface ER), and rapid chloride permeability test (RCPT). The findings emphasize the critical role of pore structure in governing chloride resistance in PLC systems. Paper 2 (Chapter 4) focuses on the chloride binding behavior of various PLC mixtures and offers new insights into the potential of high interground limestone PLC in maintaining adequate binding performance, particularly when combined with SCMs. Chapter 5 (Conclusion) summarizes the key findings of the study and proposes several future research directions to address unresolved challenges. Finally, the Appendix provides a supplementary description of the laboratory procedures used to determine total chloride and free chloride content in concrete samples.

1.3 Reference

[1] C. Li and L. Jiang, "The role of chloride binding mechanism in the interpretation of chloride profiles in concrete containing limestone powder," J. Sustain. Cem.-Based Mater., vol. 12, no. 1, pp. 24–35, Jan. 2023, doi: 10.1080/21650373.2021.2010243.

[2] "4 ways to make the cement industry more sustainable," World Economic Forum. Accessed: Apr. 05, 2025. [Online]. Available: https://www.weforum.org/stories/2024/09/cement-production-sustainable-concrete-co2-emissions/

[3] I. Al Khaffaf, R. A. Hawileh, S. Sahoo, J. A. Abdalla, and J. H. Kim, "Toward carbon- neutral construction: A review of zero-carbon concrete," J. Build. Eng., vol. 99, p. 111578, Apr. 2025, doi: 10.1016/j.jobe.2024.111578.

[4] I. Government of Canada, "Net Zero Accelerator Initiative." Accessed: Sep. 02, 2024. [Online]. Available: https://ised-isde.canada.ca/site/strategic-innovation-fund/en/net-zero-accelerator-initiative

[5] "Sustainable construction for a circular economy," Cement Association of Canada. Accessed: Apr. 06, 2025. [Online]. Available: https://cement.ca/sustainability/portland-limestone-cement/

[6] B. Lothenbach, K. Scrivener, and R. D. Hooton, "Supplementary cementitious materials," Cem. Concr. Res., vol. 41, no. 12, pp. 1244–1256, Dec. 2011, doi: 10.1016/j.cemconres.2010.12.001.

[7] Y. Zhou, B. Gencturk, K. Willam, and A. Attar, "Carbonation-Induced and Chloride-Induced Corrosion in Reinforced Concrete Structures," J. Mater. Civ. Eng., vol. 27, no. 9, p. 04014245, Sep. 2015, doi: 10.1061/(ASCE)MT.1943-5533.0001209.

[8] K. De Weerdt, W. Wilson, A. Machner, and F. Georget, "Chloride profiles – What do they tell us and how should they be used?," Cem. Concr. Res., vol. 173, p. 107287, Nov. 2023, doi: 10.1016/j.cemconres.2023.107287.

[9] K. De Weerdt, "Chloride binding in concrete: recent investigations and recognised knowledge gaps: RILEM Robert L'Hermite Medal Paper 2021," Mater. Struct., vol. 54, no. 6, pp. 1–16, Dec. 2021, doi: 10.1617/s11527-021-01793-9.

[10] CSA Group, Cementitious Materials Compendium, CSA A3000:23, Toronto, ON, Canada, 2023.

[11] K. Bharadwaj et al., "CALTRANS: Impact of the Use of Portland-Limestone Cement on Concrete Performance as Plain or Reinforced Material," Kiewit Center, Nov. 2021. doi: 10.5399/osu/1150.

[12] Portland Cement Association et al., "State-of-the-Art Report on Use of Limestone in Cements at Levels of up to 15%," Portland Cement Association, 2024. doi: 10.70909/pca.2024.SN3148.03.

Chapter 2

Background

2.1 Low-CO_2 cementitious materials

2.1.1 Portland-limestone cement (PLC)

As previously discussed, Portland-limestone cement (PLC), which incorporates interground limestone as a partial clinker replacement, can reduce CO_2 emissions by approximately 10% during the cement manufacturing process when used at a 15% replacement level [1]. As illustrated in Fig 2.1, the green-colored regions highlight areas in Canada (a) and the United States (b) where PLC has been formally accepted and integrated into construction practices, as originally proposed by [2]. Currently, the allowable limestone replacement level in both countries has been standardized at 15%, in accordance with ASTM C595-24 [3] in the U.S. and CSA A3000-23 [4] in Canada. A growing body of literature and field-based investigations has consistently demonstrated that PLC containing up to 15% limestone does not compromise concrete performance, including mechanical strength and durability, when compared to conventional Portland cement (PC) [1,5,6].

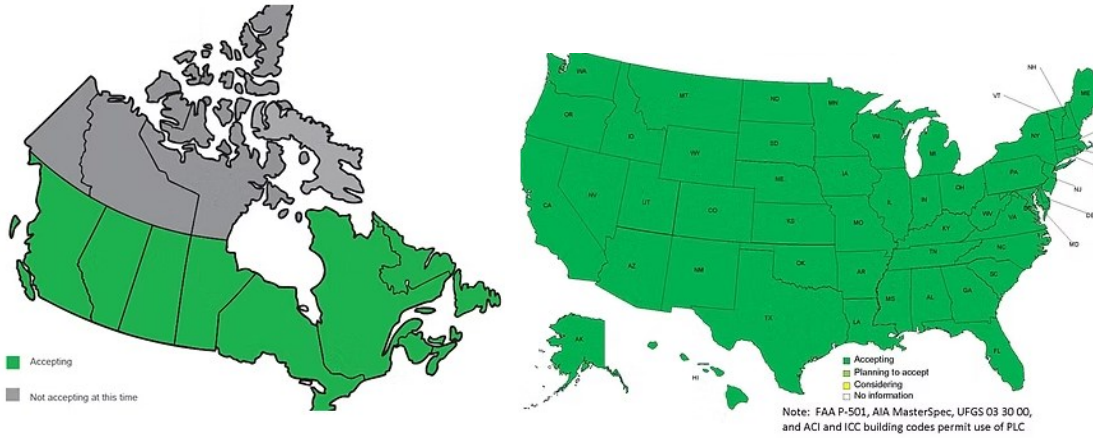

(a) (b)

Figure 2.1. PLC accepting regions (green) in Canada (a) and the US (b) [15].

2.1.2 Supplementary cementitious materials (SCMs)

Supplementary cementitious materials (SCMs), such as fly ash and slag, which are industrial by-products, are commonly used as partial replacements for Portland cement (PC) and have proven effective in significantly reducing CO_2 emissions associated with concrete production [7]. The global warming potential (GWP), an established metric for quantifying the environmental impact of construction materials, is defined as the total mass of CO_2 emitted per unit volume of concrete, as outlined in [8]. Figure 2.2 illustrates the GWP values of various binary blended cements incorporating SCMs, in comparison with conventional PC, with data compiled from [9]. The results clearly show that the inclusion of SCMs leads to substantially lower GWP values, thereby demonstrating their contribution to the development of low-carbon concrete technologies.

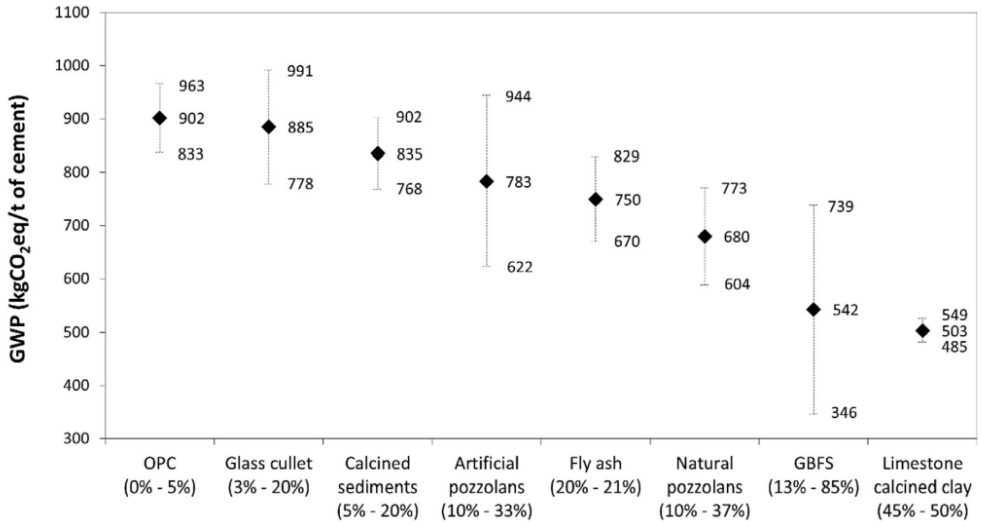

Figure 2.2**.** GWP in different cementitious materials [9].

2.2 Chloride diffusion mechanism

Diffusion is the governable transport mechanism of chloride ion ingress in concrete [10]. In this process, chloride binding capacity plays a crucial role in preventing chloride penetration and extending the initiation period of chloride-induced corrosion.

As shown in Eq (1), according to Fick's first law, the flux of chloride is independent of time.

$$Jc = -\mathrm{D}\frac{\partial \mathrm{C}}{\partial \mathrm{x}} \tag{1}$$

However, in actual concrete diffusion conditions, the diffusion is dependent on both time and depth, which is expressed as Fick's second law in Eq (2):

$$\frac{\partial C}{\partial t} = D\frac{\partial^2 C}{\partial x^2} \quad (2)$$

In the above two equations, Jc is chloride ion's flux by diffusion, kg/m^2·s, C is the chloride content, kg/m^3, x is the depth of chloride ion, m, t is the total diffusion time, s, and D is the diffusion coefficient, m^2/s.

As illustrated in Figure 2.3(a), the non-steady-state condition (represented by the dashed line) differs from the steady-state condition in that it exhibits a variable slope along the concentration profile, indicating a time-dependent diffusion process. This behavior is further reflected in Figure 2.3(b), which presents the sketch of a typical chloride concentration profile plotted as chloride content (mass % of dry concrete) versus concrete depth. The curvature of the profile highlights the influence of chloride binding, wherein the presence of binding sites within the cementitious matrix alters the effective transport of chloride ions. As binding occurs, a portion of the incoming chlorides is immobilized, causing a deviation from steady-state diffusion and resulting in a non-linear concentration gradient. This illustrates that chloride diffusion under real exposure conditions is inherently non-steady-state, particularly in materials exhibiting chloride binding capacity [11].

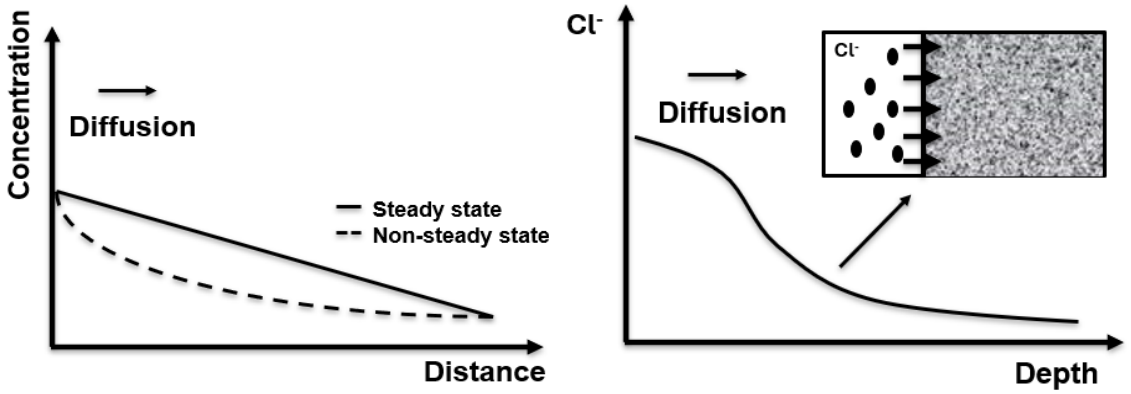

(a) (b)

Figure 2.3. Schematic of: (a) Non-steady state and steady state diffusion and (b) Typical chloride profile by diffusion.

2.3 Chloride composition in concrete

The total chloride content in concrete (expressed as a percentage of dry mass) is typically composed of three phases: chloride bound in Friedel's salt, chloride adsorbed in C-A-S-H, and free chloride ions dissolved in the pore solution. However, not all C-A-S-H phases contribute equally to chloride immobilization. De Weerdt et al. [12] identified that strongly bound chlorides, those considered immobile, are primarily stabilized within AFm interlayers (Cl-AFm) and are associated with approximately 10–20% of the C-A-S-H fraction. These strongly bound chlorides play a critical role in reducing chloride ingress and mitigating the risk of reinforcement corrosion [13]. This insight has significantly contributed to the understanding of chloride binding mechanisms and underscores the need for further research on the distinct roles of AFm and C-A-S-H phases in various cementitious systems, many of which remain insufficiently characterized.

2.4 Cementitious materials' influences on chloride resistance

Distinct cementitious materials may differently impact on chloride resistance. The influence of limestone fillers along with common supplementary cementitious materials are presented hereafter:

2.4.1 Limestone filler

Limestone fillers exhibit multifaceted effects on the chloride resistance of concrete. On the one hand, the physical filler effect of finely ground limestone improves particle packing by filling voids between cement grains, thereby increasing the overall density of the cementitious matrix [14]. Additionally, during the early stages of hydration, limestone filler particles act as nucleation sites for C-A-S-H formation, a mechanism commonly referred to as the nucleation effect [15]. Both mechanisms contribute positively to chloride resistance by refining the pore structure and enhancing the early development of hydration products.

On the other hand, excessive limestone replacement may lead to the so-called dilution effect, wherein a reduced proportion of reactive clinker results in lower overall hydration products

formation [16]. The increased presence of non-reactive fillers creates more free water in the system, ultimately reducing the volume of hydration products and compromising durability. Contrary to earlier assumptions that limestone behaves as an inert filler, substantial evidence suggests that it participates in chemical reactions with aluminates. Specifically, limestone can react with C_3A to form carboaluminate phases [17,18]. This reaction can stabilize ettringite (AFt) by consuming C_3A, thereby delaying its conversion to AFm phases [19], eventually decreasing the potential for the formation of Friedel's salt; whereas some studies have proposed that carboaluminate phases, such as monocarboaluminate (Mc) and hemicarboaluminate (Hc), can also chemically bind chloride ions [6,20]. Therefore, the chloride resistance performance of PLC concrete incorporating higher levels of interground limestone remains insufficiently understood and warrants further investigation.

2.4.2 Fly ash

Fly ash, a by-product of coal combustion, plays a significant role in influencing the chloride resistance performance of concrete. As a pozzolanic material, fly ash is characterized by a relatively low CaO content and elevated levels of SiO_2 and Al_2O_3 compared to PC [7]. Its pozzolanic activity relies on the presence of portlandite, a product of PC hydration, which reacts with the reactive silica and alumina in fly ash to form additional C-A-S-H and other secondary hydration products. This reaction contributes to densifying the microstructure and reducing permeability, thereby enhancing chloride resistance [21]. Moreover, the high Al_2O_3 content in fly ash can enhance chemical chloride binding by enriching the system with additional alumina, which promotes the transformation of ettringite (AFt) into monosulfate-type (AFm) phases. These AFm phases are capable of chemically binding chloride ions through the formation of Friedel's salt. However, the introduction of additional Al_2O_3 from fly ash in systems containing limestone fillers may intensify the stabilizing AFt and delaying the transformation to AFm, as previously discussed [19]. This, in turn, can lead to increased formation of carboaluminates, enhancing solid volume and reducing pore connectivity, which favors reduced permeability. Otherwise, it may delay the transformation from AFt to AFm,

thereby diminishing the chemical chloride binding capacity of the system. Consequently, the chloride resistance performance of concrete incorporating both limestone filler and fly ash remains complex and not yet fully understood, particularly in high-limestone PLC systems.

2.4.3 Slag

Compared to fly ash, slag generally contains a higher proportion of CaO, meaning it does not rely heavily on portlandite to initiate secondary hydration. As a result, slag can independently contribute to the formation of additional hydration products, which improve microstructural densification. Numerous studies have reported that the incorporation of slag enhances the chloride resistance of conventional concrete by reducing permeability and refining the pore structure [22-24]. However, emerging evidence from X-ray diffraction (XRD) analyses suggests a more nuanced effect when slag is blended with PC. Several studies have observed a reduction in the formation of AFt and AFm phases in slag-blended systems [25,26]. Furthermore, a significant portion of the Al_2O_3 present in slag tends to become chemically incorporated within the C-A-S-H structure rather than contributing to AFm phase formation [7].

2.4.4 Silica fume

The incorporation of silica fume into concrete mixtures has demonstrated diverse effects on chloride resistance, depending on the mechanism considered. From a microstructural perspective, silica fume significantly refines the pore structure of cement paste through its pozzolanic reaction with calcium hydroxide. This reaction leads to the formation of additional C-A-S-H, which in turn reduces the volume of capillary pores and contributes to a denser and more discontinuous pore network, thereby lowering the permeability of concrete [7]. However, when viewed from the perspective of chloride binding, silica fume generally exhibits limited direct chemical binding capacity, especially when compared to aluminum-rich SCMs such as slag and fly ash. While the increased formation of C-A-S-H may enhance physical chloride binding, the C-A-S-H generated from silica fume tends to have a lower Ca/Si ratio, which is associated with reduced chloride

binding capacity overall [27]. Consequently, although silica fume improves resistance to chloride ingress by reducing transport pathways, its contribution to chemical chloride binding is relatively modest.

2.5 Chloride-related determination

2.5.1 Chloride binding

2.5.1.1 Equilibrium method for cement paste and mortar

The equilibrium method is considered a direct and reliable technique for quantifying the bound chloride content in cement paste and mortar, offering a clear measure of chloride binding capacity [27]. This method was first introduced by Tritthart in 1988 [28], where cement paste samples with a thickness of approximately 1 cm are immersed in a chloride solution of known concentration for an extended period, typically over 380 days, until equilibrium is reached between the external solution and the pore solution within the cement matrix. Upon completion of the immersion, the amount of bound chloride is calculated by measuring the difference in chloride concentration of the external solution before and after exposure, using potentiometric titration.

Due to the limitations associated with the long duration required to reach equilibrium in Tritthart's original method, Tang and Nilsson [29] proposed a modified approach involving the use of finely ground samples (i.e., 0.25–2mm particles, approx. 25g) with pre-conditioning to accelerate ion exchange. These samples are immersed in a series of external chloride solutions of varying concentrations until equilibrium is reached, which can typically occur within 14 days. Chloride content in the solution is again determined via potentiometric titration using 0.01 M $AgNO_3$. This accelerated approach retains the accuracy of the equilibrium method while enabling more practical and timely testing in laboratory conditions.

The detailed bound chloride content calculation is shown in Eq (3):

$$C_b = 35.453 \times V \times (C_i - C_f)/W_d \quad (3)$$

Where: Cb is the bound chloride content, mg/g, V is the volume of the external chloride solution, ml, Ci is the initial chloride concentration before sample immersion, mol/l, Cf is the free chloride concentration after achieving equilibrium condition, mol/l, and Wd is the mass dry sample, g.

The same procedure has also been widely adopted in studies evaluating chloride binding capacity across different binder systems [6,30], and has been effectively integrated into service life prediction models for reinforced concrete structures exposed to chloride environments [31,32].

2.5.1.2 Total and free chloride determination for dry concrete powder

Strongly bound chloride content in the concrete of experimental studies can be estimated as the difference between acid-soluble and water-soluble chloride fractions [12]. This approach is based on the principle that both bound and free chloride ions dissolve completely in diluted nitric acid, while only the mobile (free) chloride fraction is soluble in deionized [33] or distilled water [34]. Using potentiometric titration, chloride contents can be quantitatively determined from powdered concrete samples. The reliability of this method has been validated through Round-Robin (multi-laboratory) testing, which supports the use of acid-soluble analysis for measuring total chloride [35] and water-soluble analysis for free chloride [36]. Loser et al. [37] confirmed the applicability of this methodology for comparing chloride binding capacity across various binder systems. Similar analytical techniques have also been adopted in studies investigating chloride binding under marine exposure conditions [38].

2.5.1.3 Phase composition analysis

X-ray diffraction (XRD) is a widely used analytical technique in cement chemistry for identifying crystalline hydration products and phase transformations. In the context of chloride binding, XRD enables the detection of chloride-containing phases, particularly Friedel's salt (Cl-AFm), which forms through the chemical interaction between chloride ions and aluminous hydration phases such as monosulfate. Thermogravimetric analysis (TGA) provides a complementary perspective on

chloride binding by evaluating mass loss associated with specific decomposition temperatures of cement hydration products. In chloride-exposed systems, TGA can be used to detect the thermal decomposition of Friedel's salt, depending on system chemistry. By comparing mass loss curves of samples before and after chloride exposure, researchers can infer the quantity of chemically bound chlorides and distinguish it from other phases such as portlandite, AFt, or carbonate-bearing AFm phases. Figure 2.4 presented the experimental analysis from [39].

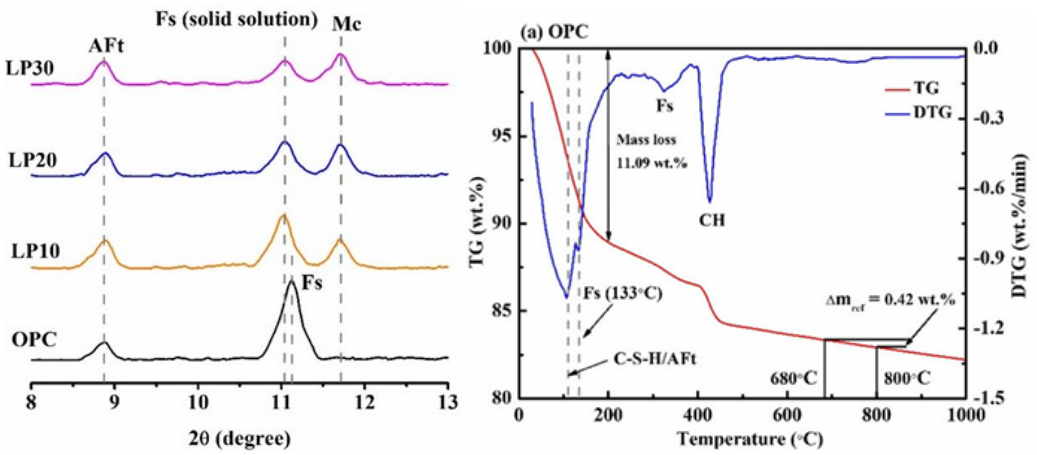

Figure 2.4. XRD and TGA analysis from [41].

2.5.1.4 Chloride binding isotherms

Chloride binding isotherms are widely employed to characterize the relationship between free chloride concentration and the amount of chloride bound within the cementitious matrix at a given temperature. These isotherms provide valuable insight into the binding behavior of concrete, which varies depending on the composition of the cementitious system [31] and significantly influences the rate of chloride ingress. As proposed by [40], chloride binding capacity can be quantified as the derivative $\partial Cb/\partial Cf$, representing the change in bound chloride with respect to free chloride concentration. Experimental data are typically fitted to empirical or semi-empirical models, including the linear, Langmuir, and Freundlich isotherms, each offering different assumptions and mechanisms for describing the interaction between chlorides and hydration products. These models

help quantify binding capacity and support a better understanding of chloride transport resistance in diverse binder systems. These three binding isotherms equations are shown hereafter:

Linear isotherm:

$$C_b = kC_f \, , \frac{\partial C_b}{\partial C_f} = k \tag{4}$$

Freundlich isotherm:

$$C_b = \alpha {C_f}^{\beta} \, , \, \frac{\partial C_b}{\partial Cf} = \alpha\beta {C_f}^{\beta-1} \tag{5}$$

Langmuir isotherm:

$$C_b = \frac{\alpha C_f}{1+\beta C_f} \, , \, \frac{\partial C_b}{\partial C_f} = \frac{\alpha}{(1+\beta C_f)^2} \tag{6}$$

In the above, Cb is the bound chloride content, Cf is the free chloride content, and α, β, and k are fitting parameters which have no physical meanings.

As discussed in [31], the linear isotherm offers a simplified approach to modeling chloride binding in cementitious materials. While it provides a convenient and intuitive approximation, it tends to underestimate bound chloride at low free chloride concentrations and overestimate it at higher concentrations. Nevertheless, a linear relationship between free and bound chlorides has been observed in long-term field exposure studies, including marine environments over a 7-year period [41].

In contrast, the Freundlich and Langmuir isotherms are more widely adopted for modeling chloride binding due to their ability to capture nonlinear behavior. According to Tang and Nilsson [29], the Freundlich model is more appropriate when the external chloride concentration exceeds 0.01 mol/L, whereas the Langmuir model offers better accuracy at concentrations below 0.05 mol/L in cement paste and mortar systems. Laboratory studies on concrete specimens, however, have demonstrated that both models remain applicable. For example, Li and Jiang [39] reported high correlation coefficients for both isotherms under a 0.6 mol/L chloride exposure over a four-month bulk diffusion test. Furthermore, a review by Song et al. [42] concluded that linear, Freundlich, and

Langmuir models have all been successfully applied to chloride binding in concrete. The use of modified fitting parameters across studies reflects the complexity of chloride binding behavior and suggests that a universally applicable model has yet to be established, especially for evaluations based on concrete specimens.

2.5.2 Experiments on chloride resistance evaluation

2.5.2.1 Bulk diffusion test

Among the primary mechanisms governing ion transport in concrete, which namely diffusion, permeation, capillary adsorption, and electromigration, diffusion is recognized as the dominant process for the natural ingress of chloride ions under typical exposure conditions [10]. To simulate this phenomenon, the bulk diffusion test, as standardized in ASTM C1556 [43], is commonly employed to evaluate non-steady-state chloride transport in concrete. As illustrated in Fig 5, the procedure involves conditioning specimens under controlled curing regimes, followed by cutting them into standardized dimensions and immersing them in a 165 g/L sodium chloride (NaCl) solution for a minimum of 35 days. After the immersion period, samples are removed, and chloride concentration profiles are obtained by analyzing powdered layers taken from incremental depths. Chloride contents can be quantified using methods such as manual or automatic potentiometric titration [37,39,44], as well as advanced techniques like inductively coupled plasma mass spectrometry (ICP-MS) [45] and micro X-ray fluorescence (μXRF) [46].

From the resulting chloride profiles, the apparent diffusion coefficient (Da) can be calculated, which serves as a critical parameter for assessing a concrete system's resistance to chloride ingress. In recent years, Da has also become a foundational input in various chloride transport and service life prediction models used in durability design for reinforced concrete infrastructure [12].

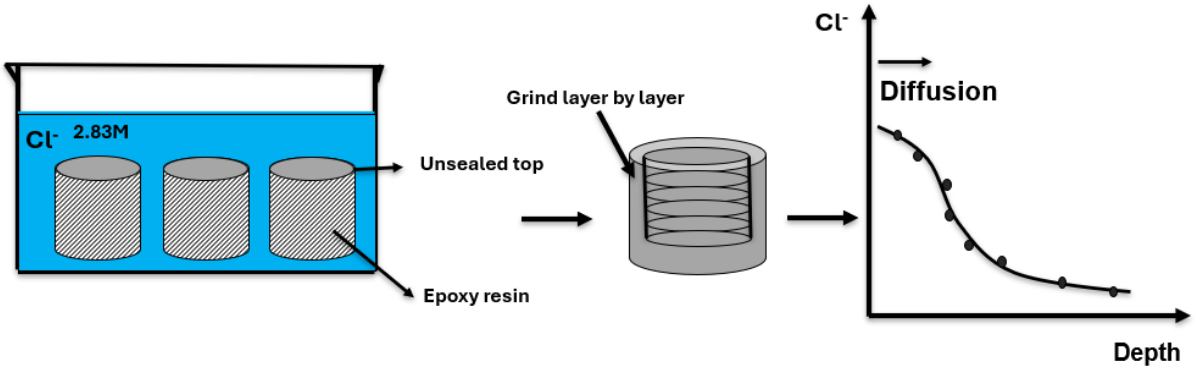

Figure 2.5. Schematic of chloride profile determination process.

2.5.2.2 Electrical resistivity test

Due to the time-consuming nature of the bulk diffusion test, requiring both an initial curing period and a minimum 35-day immersion in chloride solution, electrical resistivity tests are frequently used as indirect indicators of a concrete's chloride resistance. Unlike diffusion-based tests, resistivity measurements do not account for chloride ion transport or binding mechanisms [11]. Bulk ER is typically conducted in laboratory environments using cylindrical specimens, either extracted from field structures or cast specifically for evaluation. The measured resistivity reflects the internal microstructure and pore connectivity of the concrete. In general, lower bulk resistivity values are associated with higher permeability, indicating a greater susceptibility to moisture and chloride ingress and, thus, an elevated risk of reinforcement corrosion.

Surface ER testing has gained popularity due to its simplicity, rapid execution, and non-destructive nature. This method involves placing a four-probe array on the surface of the concrete and applying a low-voltage current across the probes at a standardized spacing. Its convenience and speed have led to widespread use for preliminary assessments of chloride resistance, particularly in field applications. The sketch of bulk ER and surface ER are displayed in Figure 2.6 (a) and (b), respectively [47].

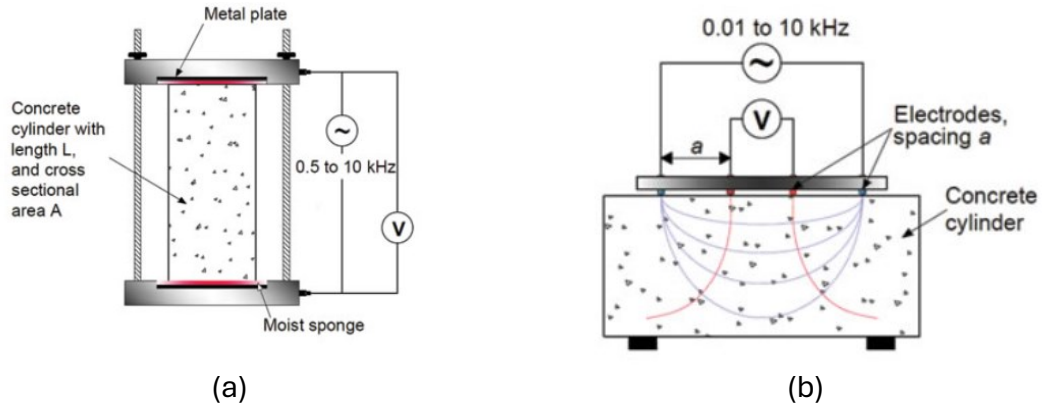

Figure 2.6. Schematic of (a) Bulk ER [47] and (b) Surface ER [47].

2.5.2.3 Chloride migration related tests

In this session, a series of main chloride migration tests under different applied voltages are summarized hereafter.

2.5.2.3.1 Rapid chloride permeability test (RCPT)

A widely used method for evaluating the chloride resistance of concrete is the rapid chloride permeability test (RCPT), standardized under ASTM C1202 [48]. In this test, a 60 V potential is applied across a saturated concrete specimen positioned between two chambers: one filled with a sodium chloride (NaCl) solution and the other with a sodium hydroxide (NaOH) solution. The total electrical charge passed through the specimen over a 6-hour period is recorded and expressed in coulombs.

RCPT offers a rapid and convenient means of assessing chloride penetration resistance. Lower charge values indicate reduced ionic transport and, by extension, higher resistance to chloride ingress, correlating with improved durability and a lower risk of reinforcement corrosion. However, while the method is favoured for its speed and simplicity, the passage of current during the test can elevate the temperature of the specimen, particularly in mixtures with lower electrical resistivity, which may artificially increase ionic mobility. As a result, RCPT outcomes can be sensitive to concrete composition and testing conditions, complicating direct comparisons between different mixtures or binder systems [49].

2.5.2.3.2 Rapid chloride migration test (RCMT)

The rapid chloride migration test (RCMT), standardized by NT BUILD 492 [53], is a widely accepted accelerated test method developed to assess the chloride ingress resistance of concrete. The specimen dimensions used for RCMT are identical to those in the RCPT, typically 100 mm in diameter and 50 mm in length, and both tests require sample preconditioning, including vacuum saturation. During RCMT, the specimen is mounted in an electrolytic cell divided into two compartments: one containing a chloride-free solution (0.3 M NaOH) and the other filled with a chloride-rich solution (10% NaCl). A direct current voltage, typically 30 V (adjusted based on the initial conductivity of the concrete), is applied across the specimen for a fixed duration, usually 24 hours. Upon completion of the migration period, the specimen is axially split, and the freshly fractured surface is sprayed with a silver nitrate ($AgNO_3$) solution. This results in a visible white precipitate (AgCl) marking the depth of chloride penetration. The chloride penetration depth is measured at multiple locations, and the average value is used to calculate the chloride migration coefficient, which serves as a performance indicator for chloride resistance.

It is worth noting that while both RCPT and RCMT are designed to simulate non-steady-state chloride transport and, to some extent, account for chloride binding, their short testing durations and high applied voltages significantly limit the extent of chloride binding that occurs during the test [37]. As a result, the outcomes primarily reflect ionic transport capacity rather than long-term binding behavior.

2.5.2.3.3 Chloride conductivity test (CC)

The rapid chloride conductivity test is a laboratory-based method developed to evaluate the resistance of concrete to chloride ingress. Initially introduced by Streicher et al. [50] and subsequently refined through further research by Otieno et al. [51], this method provides a quick and efficient means of assessing concrete's chloride transport properties. In this procedure, cylindrical concrete specimens are first oven-dried to remove moisture and then vacuum-saturated

with a high-concentration sodium chloride solution (i.e., 5M NaCl) to simulate chloride exposure conditions. Following saturation, the specimens are mounted in a custom-designed test cell composed of two compartments, both filled with the same salt solution to maintain ionic consistency. A 10 volt direct current potential is applied across the specimen, and the resulting electric current is recorded after a brief stabilization period, typically around 10 seconds. This measured current is then used to compute the chloride conductivity of the concrete, which serves as a proxy for its chloride ingress resistance. This method offers several advantages, including rapid execution, simple setup, and the ability to differentiate mixtures based on ionic transport characteristics, making it especially useful for comparative studies of concrete performance under aggressive environmental exposure.

All of the chloride migration-related tests are presented in Figure 2.7 (a) RCPT, (b) RCMT, and (c) CC.

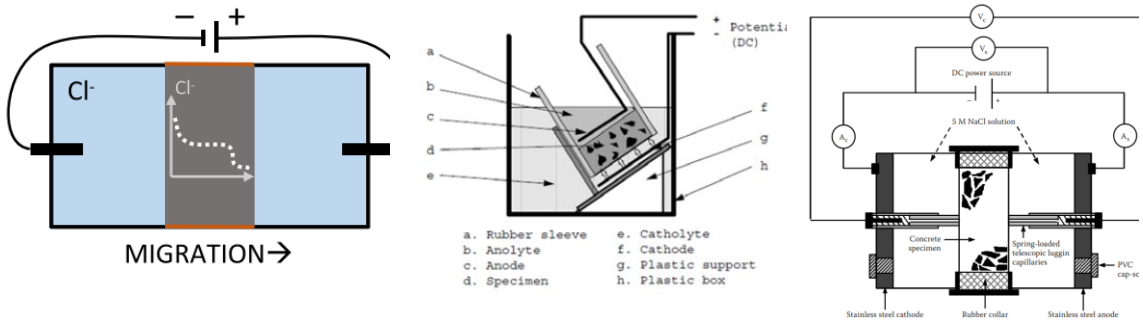

(a) (b) (c)

Figure 2.7. Schematic of chloride migration-related tests: (a) RCPT [11], (b) RCMT [52], and (c) CC [51].

2.6 Research gaps

In summary, many existing studies have focused on the individual effects of specific cementitious materials, such as limestone filler, fly ash, or other SCMs, on chloride resistance and/or chloride binding. However, the interactions between these materials within blended cement systems remain poorly understood. Furthermore, in support of achieving Net-Zero carbon emission targets, increasing the interground limestone replacement level beyond the current 15% limit in PLC systems has gained attention. This ambition, however, raises concerns regarding the long-term

durability of concrete, particularly in terms of chloride ingress resistance. Therefore, a comprehensive and systematic investigation into both the chloride resistance and chloride binding behavior of PLC concretes, especially those incorporating high levels of limestone and various SCMs, is essential to ensure the reliability and sustainability of next-generation low-carbon concrete technologies.

2.7 References

[1] "A Technical Introduction to Portland-limestone Cement for Municipal and Provincial Construction Specifications," Cement Association of Canada. Accessed: Mar. 12, 2025. [Online]. Available: https://cement.ca/expertise_center/report/introduction-to-portland-limestone-cement-for-municipal-provincial-construction/

[2] "PLC: Greener Cement | Worldwide Acceptance," Greener Cement. Accessed: Mar. 12, 2025. [Online]. Available: https://www.greenercement.com/acceptance

[3] ASTM C0595/C0595M-24, Standard Specification for Blended Hydraulic Cements. ASTM International, 2024.

[4] CSA Group, Cementitious Materials Compendium, CSA A3000:23, Toronto, ON, Canada, 2023.

[5] Portland Cement Association et al., "State-of-the-Art Report on Use of Limestone in Cements at Levels of up to 15%," Portland Cement Association, 2024. doi: 10.70909/pca.2024.SN3148.03.

[6] K. Bharadwaj et al., "CALTRANS: Impact of the Use of Portland-Limestone Cement on Concrete Performance as Plain or Reinforced Material," Kiewit Center, Nov. 2021. doi: 10.5399/osu/1150.

[7] B. Lothenbach, K. Scrivener, and R. D. Hooton, "Supplementary cementitious materials," Cem. Concr. Res., vol. 41, no. 12, pp. 1244–1256, Dec. 2011, doi: 10.1016/j.cemconres.2010.12.001.

[8] M. T. de Grazia, Short and Long-Term Performance of Eco-Efficient Concrete Mixtures, Ph.D. dissertation, Dept. of Civil Engineering, Univ. of Ottawa, Ottawa, ON, Canada, 2023. [Online]. Available: https://ruor.uottawa.ca/items/59f624ec-b630-4d40-9069-e7e773686ab3.

[9] Y. Rhaouti, Y. Taha, and M. Benzaazoua, "Assessment of the Environmental Performance of Blended Cements from a Life Cycle Perspective: A Systematic Review," Sustain. Prod. Consum., vol. 36, pp. 32–48, Mar. 2023, doi: 10.1016/j.spc.2022.12.010.

[10] Z. Xu and G. Ye, “Understanding Chloride Diffusion Coefficient in Cementitious Materials,” Materials, vol. 16, no. 9, Art. no. 9, Jan. 2023, doi: 10.3390/ma16093464.

[11] W. Wilson, F. Georget, and K. Scrivener, “Unravelling chloride transport/microstructure relationships for blended-cement pastes with the mini-migration method,” Cem. Concr. Res., vol. 140, p. 106264, Feb. 2021, doi: 10.1016/j.cemconres.2020.106264.

[12] K. De Weerdt, W. Wilson, A. Machner, and F. Georget, “Chloride profiles – What do they tell us and how should they be used?,” Cem. Concr. Res., vol. 173, p. 107287, Nov. 2023, doi: 10.1016/j.cemconres.2023.107287.

[13] Chloride penetration into concrete, State-of-the-Art. Transport processes, corrosion initiation, test methods and prediction models,” ResearchGate. Accessed: Mar. 13, 2025. [Online]. Available: https://www.researchgate.net/publication/264420368_HETEK_Chloride_penetration_into_concrete_State-of-the-Art_Transport_processes_corrosion_initiation_test_methods_and_prediction_models

[14] D. Wang, C. Shi, N. Farzadnia, Z. Shi, H. Jia, and Z. Ou, “A review on use of limestone powder in cement-based materials: Mechanism, hydration and microstructures,” Constr. Build. Mater., vol. 181, pp. 659–672, Aug. 2018, doi: 10.1016/j.conbuildmat.2018.06.075.

[15] Y. Briki, M. Zajac, M. B. Haha, and K. Scrivener, “Impact of limestone fineness on cement hydration at early age,” Cem. Concr. Res., vol. 147, p. 106515, Sep. 2021, doi: 10.1016/j.cemconres.2021.106515.

[16] A. C. Bergmann et al., “Influence of Interparticle Separation Distance on the Fresh and Hardened Behavior of Ecoefficient Cement Pastes,” J. Mater. Civ. Eng., vol. 35, no. 8, p. 04023252, Aug. 2023, doi: 10.1061/JMCEE7.MTENG-14988.

[17] G. Kakali, S. Tsivilis, E. Aggeli, and M. Bati, “Hydration products of C3A, C3S and Portland cement in the presence of CaCO3,” Cem. Concr. Res., vol. 30, no. 7, pp. 1073–1077, Jul. 2000, doi: 10.1016/S0008-8846(00)00292-1.

[18] G. Menéndez, V. Bonavetti, and E. F. Irassar, “Strength development of ternary blended cement with limestone filler and blast-furnace slag,” Cem. Concr. Compos., vol. 25, no. 1, pp. 61–67, Jan. 2003, doi: 10.1016/S0958-9465(01)00056-7.

[19] K. De Weerdt, K. O. Kjellsen, E. Sellevold, and H. Justnes, “Synergy between fly ash and limestone powder in ternary cements,” Cem. Concr. Compos., vol. 33, no. 1, pp. 30–38, Jan. 2011, doi: 10.1016/j.cemconcomp.2010.09.006.

[20] K. De Weerdt, “Chloride binding in concrete: recent investigations and recognised knowledge gaps: RILEM Robert L’Hermite Medal Paper 2021,” Mater. Struct., vol. 54, no. 6, pp. 1–16, Dec. 2021, doi: 10.1617/s11527-021-01793-9.

[21] M. T. De Grazia, H. Deda, and L. F.M. Sanchez, “The influence of the binder type & aggregate nature on the electrical resistivity of conventional concrete,” J. Build. Eng., vol. 43, p. 102540, Nov. 2021, doi: 10.1016/j.jobe.2021.102540.

[22] H. Yildirim, T. Ilica, and O. Sengul, “Effect of cement type on the resistance of concrete against chloride penetration,” Constr. Build. Mater., vol. 25, no. 3, pp. 1282–1288, Mar. 2011, doi: 10.1016/j.conbuildmat.2010.09.023.

[23] D. G. Mapa, H. Zhu, F. Nosouhian, N. Shanahan, K. A. Riding, and A. Zayed, “Chloride binding and diffusion of slag blended concrete mixtures,” Constr. Build. Mater., vol. 388, p. 131584, Jul. 2023, doi: 10.1016/j.conbuildmat.2023.131584.

[24] A. Runci, J. Provis, and M. Serdar, “Microstructure as a key parameter for understanding chloride ingress in alkali-activated mortars,” Cem. Concr. Compos., vol. 134, p. 104818, Nov. 2022, doi: 10.1016/j.cemconcomp.2022.104818.

[25] R. Taylor, I. G. Richardson, and R. M. D. Brydson, “Composition and microstructure of 20-year-old ordinary Portland cement–ground granulated blast-furnace slag blends containing 0 to 100% slag,” Cem. Concr. Res., vol. 40, no. 7, pp. 971–983, Jul. 2010, doi: 10.1016/j.cemconres.2010.02.012.

[26] K. A. Snyder, P. E. Stutzman, J. Philip, and D. Esh, “HYDRATED PHASES IN BLENDED CEMENTITIOUS SYSTEMS FOR NUCLEAR INFRASTRUCTURE”, 2013

[27] Q. Yuan, C. Shi, G. De Schutter, K. Audenaert, and D. Deng, “Chloride binding of cement-based materials subjected to external chloride environment – A review,” Constr. Build. Mater., vol. 23, no. 1, pp. 1–13, Jan. 2009, doi: 10.1016/j.conbuildmat.2008.02.004.

[28] J. Tritthart, “Chloride binding in cement II. The influence of the hydroxide concentration in the pore solution of hardened cement paste on chloride binding,” Cem. Concr. Res., vol. 19, no. 5, pp. 683–691, Sep. 1989, doi: 10.1016/0008-8846(89)90039-2.

[29] T. Luping and L.-O. Nilsson, “Chloride binding capacity and binding isotherms of OPC pastes and mortars,” Cem. Concr. Res., vol. 23, no. 2, pp. 247–253, Mar. 1993, doi: 10.1016/0008-8846(93)90089-R.

[30] M. D. A. Thomas, R. D. Hooton, A. Scott, and H. Zibara, “The effect of supplementary cementitious materials on chloride binding in hardened cement paste,” Cem. Concr. Res., vol. 42, no. 1, pp. 1–7, Jan. 2012, doi: 10.1016/j.cemconres.2011.01.001.

[31] B. Martín-Pérez, H. Zibara, R. D. Hooton, and M. D. A. Thomas, “A study of the effect of chloride binding on service life predictions,” Cem. Concr. Res., vol. 30, no. 8, pp. 1215–1223, Aug. 2000, doi: 10.1016/S0008-8846(00)00339-2.

[32] V. Baroghel-Bouny, X. Wang, M. Thiery, M. Saillio, and F. Barberon, “Prediction of chloride binding isotherms of cementitious materials by analytical model or numerical

inverse analysis," Cem. Concr. Res., vol. 42, no. 9, pp. 1207–1224, Sep. 2012, doi: 10.1016/j.cemconres.2012.05.008.

[33] ASTM C1218/C1218M-20, Standard Test Method for Water-Soluble Chloride in Mortar and Concrete, ASTM International, 2020.

[34] RILEM TC 178-TMC, "RILEM TC 178-TMC: 'Testing and modelling chloride penetration in concrete'Analysis of water soluble chloride content in concrete," Mater. Struct., vol. 35, no. 253, pp. 586–588, Sep. 2002, doi: 10.1617/13841.

[35] M. Castellote and C. Andrade, "Round-Robin test on chloride analysis in concrete—Part I: Analysis of total chloride content," Mater. Struct., vol. 34, no. 9, pp. 532–549, Nov. 2001, doi: 10.1007/BF02482181.

[36] M. Castellote and C. Andrade, "Round-robin test on chloride analysis in concrete — Part II: Analysis of water soluble chloride content," Mater. Struct., vol. 34, no. 10, pp. 589–596, Dec. 2001, doi: 10.1007/BF02482124.

[37] R. Loser, B. Lothenbach, A. Leemann, and M. Tuchschmid, "Chloride resistance of concrete and its binding capacity – Comparison between experimental results and thermodynamic modeling," Cem. Concr. Compos., vol. 32, no. 1, pp. 34–42, Jan. 2010, doi: 10.1016/j.cemconcomp.2009.08.001.

[38] Y. Wang, C. Liu, Y. Tan, Y. Wang, and Q. Li, "Chloride binding capacity of green concrete mixed with fly ash or coal gangue in the marine environment," Constr. Build. Mater., vol. 242, p. 118006, May 2020, doi: 10.1016/j.conbuildmat.2020.118006.

[39] C. Li and L. Jiang, "The role of chloride binding mechanism in the interpretation of chloride profiles in concrete containing limestone powder," J. Sustain. Cem.-Based Mater., vol. 12, no. 1, pp. 24–35, Jan. 2023, doi: 10.1080/21650373.2021.2010243.

[40] L. O. Nilsson, M. Massat, and L. Tang, "Effect of Non-Linear Chloride Binding on the Prediction of Chloride Penetration Into Concrete Structures", Accessed: Mar. 15, 2025. [Online]. Available: https://www.concrete.org/publications/internationalconcreteabstractsportal.aspx?m=details&id=4554

[41] T. Cheewaket, C. Jaturapitakkul, and W. Chalee, "Long term performance of chloride binding capacity in fly ash concrete in a marine environment," Constr. Build. Mater., vol. 24, no. 8, pp. 1352–1357, Aug. 2010, doi: 10.1016/j.conbuildmat.2009.12.039.

[42] C. Song, C. Jiang, X.-L. Gu, Q. Zhang, and W.-P. Zhang, "Calibration analysis of chloride binding capacity for cement-based materials under various exposure conditions," Constr. Build. Mater., vol. 314, p. 125588, Jan. 2022, doi: 10.1016/j.conbuildmat.2021.125588.

[43] ASTM C1556-22, Standard Test Method for Determining the Apparent Chloride Diffusion Coefficient of Cementitious Mixtures by Bulk Diffusion, ASTM International, 2022.

[44] M. Thomas and T. Bremner, “Performance of lightweight aggregate concrete containing slag after 25years in a harsh marine environment,” Cem. Concr. Res., vol. 42, no. 2, pp. 358–364, Feb. 2012, doi: 10.1016/j.cemconres.2011.10.009.

[45] M. Bonta, A. Eitzenberger, S. Burtscher, and A. Limbeck, “Quantification of chloride in concrete samples using LA-ICP-MS,” Cem. Concr. Res., vol. 86, pp. 78–84, Aug. 2016, doi: 10.1016/j.cemconres.2016.05.002.

[46] W. Wilson, F. Georget, and K. L. Scrivener, “XCr/ √t as an Indicator of the Resistance Against Bulk Chloride Diffusion,” in International RILEM Conference on Synergising Expertise towards Sustainability and Robustness of Cement-based Materials and Concrete Structures, Springer, Cham, 2023, pp. 658–666. doi: 10.1007/978-3-031-33211-1_59.

[47] I. Mariani, “Evaluating Concrete Quality with Electrical Resistivity Test,” Giatec Scientific Inc. Accessed: Apr. 07, 2025. [Online]. Available: https://www.giatecscientific.com/education/evaluating-concrete-quality-with-electrical-resistivity/

[48] ASTM C1202-22, Standard Test Method for Electrical Indication of Concrete’s Ability to Resist Chloride Ion Penetration, 2022.

[49] Y. A. Villagrán-Zaccardi and C. Andrade, “Chloride ingress rate and threshold content, as determined by the ‘Integral’ test method, in concrete with several w/c ratios in saturated and unsaturated conditions,” Dev. Built Environ., vol. 8, p. 100062, Sep. 2021, doi: 10.1016/j.dibe.2021.100062.

[50] P. E. Streicher and M. G. Alexander, “A chloride conduction test for concrete,” Cem. Concr. Res., vol. 25, no. 6, pp. 1284–1294, Aug. 1995, doi: 10.1016/0008-8846(95)00121-R.

[51] Chloride conductivity testing of concrete - Past and recent developments,” ResearchGate, Oct. 2024, Accessed: Apr. 14, 2025. [Online]. Available: https://www.researchgate.net/publication/292161503_Chloride_conductivity_testing_of_concrete_-_Past_and_recent_developments

[52] Use of Concrete as the Primary Construction Material for the Pelamis Wave Energy Converter,” in ResearchGate, doi: 10.1201/b18973-44.

[53] NORDTEST, Concrete, Mortar and Cement-Based Repair Materials: Chloride Migration Coefficient from Non-Steady-State Migration Experiments, NT BUILD 492, Espoo, Finland, Nov. 1999.

Chapter 3

Evaluation of Chloride Resistance in High Interground Limestone Portland-Limestone Cement (PLC) Concrete

3.1 Abstract

Concrete production is a major contributor to global CO_2 emissions, primarily due to Portland cement (PC). Portland-limestone cement (PLC), which replaces part of the clinker with interground limestone, and the incorporation of supplementary cementitious materials (SCMs) such as fly ash and slag, offer promising low-carbon alternatives. However, the durability of high-limestone PLC remains uncertain, particularly regarding chloride ingress resistance. This study evaluates the chloride resistance of PLC concretes with various limestone replacements, incorporating different SCMs through multiple test methods. Results show that SCMs significantly improve chloride resistance under distinct PLC mixtures. A strong correlation between resistivity and apparent diffusion coefficient (Da) confirms the role of pore structure in chloride transport. However, RCPT failed to detect differences among pure PLC mixtures with varying limestone content, indicating limitations in its sensitivity for low-resistivity systems. These findings highlight the importance of using multiple evaluation methods and suggest that high-limestone PLC, when properly combined with SCMs and a better-controlled water-to-clinker ratio, can maintain sufficient durability for chloride exposure conditions.

Keywords: Portland-limestone cement (PLC), Chloride resistance, fly ash, slag.

3.2 Introduction

Concrete is the second most consumed material globally, following only water [1]. It is responsible for approximately 8% of global CO_2 emissions, and a major contributor to its environmental impact is Portland cement (PC), which is due to its energy-intensive manufacturing process [2,3]. To support carbon reduction strategies, including national goals such as Canada's Net-Zero Emissions

initiative, the development of low-carbon cement systems is essential. Promising approaches include the use of Portland-limestone cement (PLC), which incorporates interground limestone to partially replace clinker [4,5], and the blending of supplementary cementitious materials (SCMs), such as fly ash and slag, into the cementitious system [6–8]. Both methods contribute to a reduction in clinker content, thus lowering CO_2 emissions.

One of the most critical durability concerns in reinforced concrete structures is chloride-induced corrosion. Chloride ions originating from external sources, such as de-icing salts and seawater, can ingress into the concrete matrix, reach the embedded reinforcement, and initiate corrosion processes that compromise structural integrity [9,10]. Consequently, evaluating the chloride resistance of concrete is essential for predicting the corrosion initiation period and extending the service life of reinforced concrete infrastructure.

Chloride resistance is governed by two primary mechanisms: chloride binding and the pore structure of concrete. Chloride binding refers to the capacity of cement hydration products to immobilize chloride ions either chemically or physically. Chemically, chlorides can bind with aluminous hydrates such as AFm phases to form Friedel's salt, while physical binding occurs through adsorption onto the calcium aluminosilicate hydrates (C-A-S-H) gel structure [11–15]. Meanwhile, pore structure of concrete relates to the transport characteristics of the concrete microstructure, including porosity, pore connectivity, and tortuosity. Both mechanisms play integral roles in slowing chloride ingress and improving long-term durability.

Several standardized methods are employed to assess chloride resistance in concrete. The bulk diffusion test (ASTM C1556) simulates natural, non-steady-state chloride penetration over extended durations, providing reliable long-term data [16]. However, due to time constraints, accelerated electrical methods are often used in practice. These include bulk electrical resistivity (Bulk ER) and surface electrical resistivity (Surface ER) tests, both of which serve as indirect indicators of concrete pore structure. Higher resistivity values are typically associated with reduced

chloride ingress. Threshold values for interpreting Bulk ER and Surface ER in terms of chloride penetrability levels have been documented in prior literature [17,18]. Another commonly used method is the rapid chloride permeability test (RCPT) as specified in ASTM C1202, which applies a 60 V potential to measure ionic transport through concrete specimens and provides a quick estimation of chloride resistance [19].

According to CSA A3000-23 specifications, the maximum allowable interground limestone content in PLC is 15%. Extensive research has demonstrated that PLCs containing up to 15% limestone do not compromise the fresh, mechanical, or durability properties of concrete, including chloride resistance, when compared to conventional PC concrete [20–22]. However, in pursuit of deeper decarbonization, there is increasing interest in further reducing clinker content by increasing limestone replacement. While such mixtures offer improved sustainability, concerns remain regarding their long-term performance, particularly in chloride-exposed environments. Therefore, comprehensive evaluation using multiple test methods is necessary to assess the chloride resistance of high-limestone PLC systems and ensure their suitability for durable, low-carbon concrete infrastructure.

3.3 Background

3.3.1 Cementitious materials' influences on chloride resistance

Distinct cementitious materials may differently impact on chloride resistance. The influence of limestone fillers along with common supplementary cementitious materials are presented hereafter:

3.3.1.1 Limestone filler

Limestone fillers exhibit multifaceted effects on the chloride resistance of concrete. On the one hand, the physical filler effect of finely ground limestone improves particle packing by filling voids between cement grains, thereby increasing the overall density of the cementitious matrix [23]. Additionally, during the early stages of hydration, limestone filler particles act as nucleation sites

for C-A-S-H formation, a mechanism commonly referred to as the nucleation effect [24]. Both mechanisms contribute positively to chloride resistance by refining the pore structure and enhancing the early development of hydration products.

On the other hand, excessive limestone replacement may lead to the so-called dilution effect, wherein a reduced proportion of reactive clinker results in lower overall hydration products formation [25]. The increased presence of non-reactive fillers creates more free water in the system, ultimately reducing the volume of hydration products and compromising durability [23]. Contrary to earlier assumptions that limestone behaves as an inert filler, substantial evidences suggest that it participates in chemical reactions with aluminates. Specifically, limestone can react with C_3A to form carboaluminate phases [26,27]. This reaction can stabilize ettringite (AFt) by consuming C_3A, thereby delaying its conversion to AFm phases [28], eventually decreasing the potential for the formation of Friedel's salt; whereas some studies have proposed that carboaluminate phases, such as monocarboaluminate (Mc) and hemicarboaluminate (Hc), can also chemically bind chloride ions [21,29]. Therefore, the chloride resistance performance of PLC concrete incorporating higher levels of interground limestone remains insufficiently understood and warrants further investigation.

3.3.1.2 Fly ash

Fly ash, a by-product of coal combustion, plays a significant role in influencing the chloride resistance performance of concrete. As a pozzolanic material, fly ash is characterized by a relatively low CaO content and elevated levels of SiO_2 and Al_2O_3 compared to PC [31]. Its pozzolanic activity relies on the presence of portlandite, a product of PC hydration, which reacts with the reactive silica and alumina in fly ash to form additional C-A-S-H and other secondary hydration products. This reaction contributes to densifying the microstructure and reducing permeability, thereby enhancing chloride resistance [32]. Moreover, the high Al_2O_3 content in fly ash can enhance chemical chloride binding by enriching the system with additional alumina, which promotes the transformation of ettringite (AFt) into monosulfate-type (AFm) phases. These AFm phases are capable of chemically

binding chloride ions through the formation of Friedel's salt. However, the introduction of additional Al_2O_3 from fly ash in systems containing limestone fillers may intensify the stabilizing AFt and delaying the transformation to AFm, as previously discussed [28]. This, in turn, can lead to increased formation of carboaluminates, enhancing solid volume and reducing pore connectivity, which favors reduced permeability. Otherwise, it may delay the transformation from AFt to AFm, thereby diminishing the chemical chloride binding capacity of the system. Consequently, the chloride resistance performance of concrete incorporating both limestone filler and fly ash remains complex and not yet fully understood, particularly in high-limestone PLC systems.

3.3.1.3 Slag

Compared to fly ash, slag generally contains a higher proportion of CaO, meaning it does not rely heavily on portlandite to initiate secondary hydration. As a result, slag can independently contribute to the formation of additional hydration products, which improve microstructural densification. Numerous studies have reported that the incorporation of slag enhances the chloride resistance of conventional concrete by reducing permeability and refining the pore structure [33–35]. However, emerging evidence from X-ray diffraction (XRD) analyses suggests a more nuanced effect when slag is blended with PC. Several studies have observed a reduction in the formation of AFt and AFm phases in slag-blended systems [36,37]. Furthermore, a significant portion of the Al_2O_3 present in slag tends to become chemically incorporated within the C-A-S-H structure rather than contributing to AFm phase formation [31].

These findings raise concerns regarding the combined use of slag and limestone filler in PLC systems. Since limestone preferentially stabilizes AFt and delays its transformation into chloride-binding AFm phases, the reduced availability of reactive alumina from slag may exacerbate this effect. This could lead to a further decline in chemical chloride binding capacity and harm the general chloride resistance performance.

3.3.2 Experiments to assess chloride resistance

3.3.2.1 Bulk diffusion test

Among the primary transport mechanisms for ions in concrete (i.e., diffusion, permeability, capillary adsorption, and migration), diffusion is widely recognized as the dominant process governing the natural ingress of chloride ions [38]. To simulate this mechanism under non-steady-state conditions, the bulk diffusion test prescribed in ASTM C1556 is commonly employed [16]. According to the standard, after a designated curing period, concrete specimens are cut to specific dimensions and immersed in a 165 g/L sodium chloride (NaCl) solution for a minimum duration of 35 days. Upon completion of the exposure period, specimens are extracted, and the internal chloride concentration profile is determined. This is typically achieved using conventional techniques such as manual or automated potentiometric titration [11,30,39], or more advanced methods including inductively coupled plasma mass spectrometry (ICP-MS) [40] and micro X-ray fluorescence (μXRF) [41].

These measurements enable the calculation of the apparent chloride diffusion coefficient (Da), a critical parameter for evaluating a concrete's resistance to chloride ingress. In recent years, Da has also been integrated into service life prediction models and performance-based durability assessments for chloride-exposed structures [15].

3.3.2.2 Electrical resistivity test

Due to the time-consuming nature of the bulk diffusion test, requiring both an initial curing period and a minimum 35-day immersion in chloride solution, electrical resistivity tests are frequently used as indirect indicators of a concrete’s chloride resistance. Unlike diffusion-based tests, resistivity measurements do not account for chloride ion transport or binding mechanisms [13]. Bulk ER is typically conducted in laboratory environments using cylindrical specimens, either extracted from field structures or cast specifically for evaluation. The measured resistivity reflects the internal microstructure and pore connectivity of the concrete. In general, lower bulk resistivity

values are associated with higher permeability, indicating a greater susceptibility to moisture and chloride ingress and, thus, an elevated risk of reinforcement corrosion.

Surface ER testing has gained popularity due to its simplicity, rapid execution, and non-destructive nature. This method involves placing a four-probe array on the surface of the concrete and applying a low-voltage current across the probes at a standardized spacing. Its convenience and speed have led to widespread use for preliminary assessments of chloride resistance, particularly in field applications.

3.3.2.3 Rapid chloride permeability test (RCPT)

Another widely used method for evaluating the chloride resistance of concrete is the Rapid Chloride Permeability Test (RCPT), standardized under ASTM C1202-22 [19]. In this test, a 60 V potential is applied across a saturated concrete specimen positioned between two chambers: one filled with a sodium chloride (NaCl) solution and the other with a sodium hydroxide (NaOH) solution. The total electrical charge passed through the specimen over a 6-hour period is recorded and expressed in coulombs.

RCPT offers a rapid and convenient means of assessing chloride penetration resistance. Lower charge values indicate reduced ionic transport and, by extension, higher resistance to chloride ingress, correlating with improved durability and a lower risk of reinforcement corrosion. However, while the method is favoured for its speed and simplicity, the passage of current during the test can elevate the temperature of the specimen, particularly in mixtures with lower electrical resistivity, which may artificially increase ionic mobility. As a result, RCPT outcomes can be sensitive to concrete composition and testing conditions, complicating direct comparisons between different mixtures or binder systems [43].

Table 3.1. shows a summarization of the chloride ion's penetrability in different tests as aforementioned by following the existing standard.

Table 3.1. Summary of distinct accelerated chloride testing method.

Chloride penetrability	**Bulk ER (Ω·m) [17] 100-by-200-mm**	**Surface ER (KΩ·cm) [18] 100-by-200-mm**	**RCPT [17]**
High	<50	<12	>4000
Moderate	50-100	12-21	2000-4000
Low	100-200	21-37	1000-2000
Very low	200-2000	37-254	100-1000
Negligible	>2000	>254	<100

3.4 Scope of the work

According to current CSA A3000 specifications, the maximum allowable limestone replacement in PLC is 15% by mass of clinker. Extensive research has shown that PLC with 15% limestone does not compromise chloride resistance compared to PC. However, in light of growing demands for carbon footprint reduction, the potential to increase limestone content beyond this threshold introduces new challenges regarding durability, particularly resistance to chloride ingress. This study aims to enhance the understanding of chloride resistance in PLC concrete systems incorporating increased limestone replacement levels combined with supplementary cementitious materials.

3.5 Materials & Methods

3.5.1 Raw materials

The experimental variables included three levels of limestone replacement in PLC: one within the current CSA A3000 allowable limit of 15% (denoted as A), and two exceeding this threshold (H1 and H2), both containing over 20% interground limestone, with H2 having a slightly higher replacement level than H1. In addition, two types of supplementary cementitious materials (SCMs) were incorporated in selected mixtures: Type-F fly ash and slag. A natural sand with a maximum size of 4.75 mm and coarse limestone aggregate with sizes from 4.75 to 19mm were used in this

study. Figure 3.1 shows the cumulative particle size distribution of the distinct cementitious material. Table 3.2 illustrates the chemical composition of the various cementitious materials.

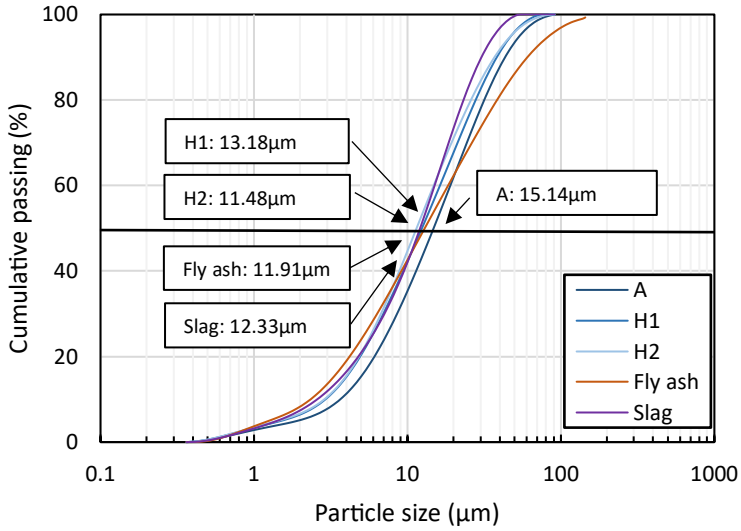

Figure 3.1. Particle size distribution of each cementitious material.

Table 3.2.Chemical composition of each cementitious material.

Mass (%)	**A**	**H1**	**H2**	**Slag**	**Fly ash**
CaO	62.19	60.83	60.87	41.45	14.22
SiO_2	18.71	17.71	17.20	36.52	49.27
Al_2O_3	4.51	4.27	4.09	10.54	16.24
Fe_2O_3	2.78	2.60	2.55	0.46	6.15
MgO	2.19	2.11	2.05	7.85	4.13
SO_3	2.95	4.62	4.42	0.24	0.68
K_2O	1.04	0.96	1.00	0.52	1.54
Na_2O	0.29	0.26	0.23	0.33	3.88
TiO_2	0.19	0.19	0.17	0.44	0.77
P_2O_5	0.13	0.13	0.12	0.00	0.40
MnO	0.06	0.05	0.06	0.29	0.06
LOI	6.23	9.217	10.05	1.36	1.29
$CaCO_3$	13.34	21.39	22.47	-	-

As shown in Table 3.2, the chemical compositions of the three types of PLC cement, as determined by XRF analysis, reveal some unexpected trends. Notably, although cement H1 and H2 both contain high levels of interground limestone, with H2 exhibiting a slightly higher $CaCO_3$ content

than H1 (i.e., 22.47 and 21.39, respectively), the measured CaO and K_2O contents in H2 are also slightly higher than those in H1. This is counterintuitive, as increased limestone replacement is expected to reduce the overall CaO content, given the lower reactivity of limestone compared to clinker. Additionally, SO_3 content, which primarily originates from gypsum rather than clinker phases, should remain relatively consistent across these cements, since limestone only partially replaces clinker. However, a significant variation in SO_3 levels is observed, further suggesting inconsistencies in the manufacturing process.

3.5.2 Mix proportions

A water-to-powder ratio (W/P) of 0.4 in accordance with the class C-1 exposure condition in CSA A23.1 [44] was selected for this research, and the concrete mixtures were proportioned via the ACI method. High-range (HR) and mid-range (MR) water-reducing admixtures were added by mass of total powder in the mix to achieve ideal workability, and an air-entrainer admixture was added to the mix to provide 5-8% of air in accordance with the C-1 exposure condition requirement for preventing freezing and thawing cycles.

The detailed mix proportions are shown in Table 3.3. Fly ash and slag were marked as “F” and “S”, and each number followed by the abbreviation represents the replacement level of that specific cementitious material. For instance, “AF20” represents cement A + 20% fly ash blended in this powder system.

Table 3.3. Mix proportions.

Mixture name	W/P	Cement (kg/m^3)	SCMs* (kg/m^3)	Fine aggregate (kg/m^3)	Coarse aggregate (kg/m^3)	HR (kg/m^3)	MR (kg/m^3)	Air content** (%)
A	0.4	326	-	866	1179	3.26	3.26	5.7
H1	0.4	326	-	866	1179	3.26	3.26	5.5
H2	0.4	326	-	866	1179	3.26	3.26	5.9
AF20	0.4	261	65	866	1179	2.28	2.28	6.3
AF40	0.4	196	130	866	1179	2.28	2.28	6.6
H1F20	0.4	261	65	866	1179	2.28	2.28	7.1
H1F40	0.4	196	130	866	1179	2.28	2.28	6.8
H2F20	0.4	261	65	866	1179	2.28	2.28	7.1
H2F40	0.4	196	130	866	1179	2.28	2.28	6.2
AS20	0.4	261	65	866	1179	2.61	2.61	7.4
AS40	0.4	196	130	866	1179	2.61	2.61	6.8
H1S20	0.4	261	65	866	1179	2.61	2.61	7.5
H1S40	0.4	196	130	866	1179	2.61	2.61	6.8
H2S20	0.4	261	65	866	1179	2.61	2.61	6.1
H2S40	0.4	196	130	866	1179	2.61	2.61	6.8

*SCMs indicate fly ash or slag in accordance with the different mixture names.
**All the mixtures were air-entrained by adding air-entrainer followed by C-1 exposure; the air content of fresh state ranges from 5-8%.

3.5.3 Samples fabrication and curing process

Three test samples (100 mm in diameter, 200 mm in length) per family were cast and stored at 21 ± 1°C with over 90% relative humidity (RH) for 24 hours. After demolding, all the samples were cured in saturated calcium hydroxide water for 56 days to reduce the influence of hydration on the test outcomes. After curing, all the samples were prepared and tested in bulk and surface ER, along with rapid chloride permeability test and bulk diffusion tests.

3.5.4 Bulk electrical resistivity test

The bulk electrical resistivity (Bulk ER) test was conducted according to ASTM C1876 [45]and CSA A23.3 - 26C [17]. As Figure 3.2 shows, two electrodes were placed on each cylinder's surface

with moist sponges for connection. After applying the required voltage potential, the resistance of the material was computed. The Bulk ER was then calculated using the following equation:

$$\rho = R * \frac{A}{L} \quad (1)$$

Where ρ is bulk ER, Ω·m. R is the electrical resistance calculated by the setup, Ω. A is the cylinder's area, which is attached to the electrode, m^2. L is the total length of the concrete cylinder, m.

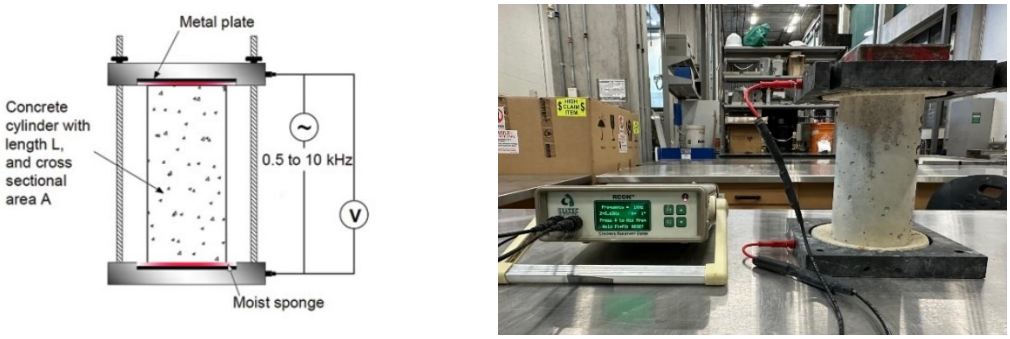

(a) (b)

Figure 3.2. Bulk ER: (a) Schematic [46] and (b) Experiments in the laboratory.

3.5.5 Surface electrical resistivity test

The surface electrical resistivity (Surface ER) was performed following AASHTO TP-95 [18]. Two inner probes were used to detect the voltage potential (V), and the two exterior probes were used to measure the current (A), as per Figure 3.3(a). The surface ER was then calculated through the following equation:

$$\rho = 2a\pi R \quad (2)$$

Where: ρ is surface ER, KΩ·cm. a is the distance of each two probes, and R is the surface resistance measured by the setup, KΩ.

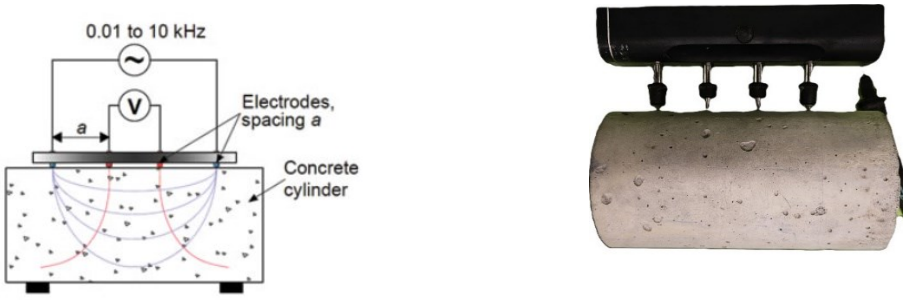

(a) (b)

Figure. 3.3. Surface ER: (a) Schematic [46] and (b) Experiments in the laboratory.

3.5.6 Rapid chloride permeability test (RCPT)

RCPT was performed following ASTM C1202-22 [19]. After curing period, a water-cooled diamond saw was used to cut the samples to a specific dimension, 100 mm in diameter, 50 mm in length. Then, the specimens were placed into a stainless-steel container, sealed with an acrylic lid and left under vacuum for three hours. Next, the samples were put back under vacuum for a supplementary hour. After a total soaking period of twenty hours, the samples were placed into an acrylic-made cell, and a 3% NaCl and 0.3 N NaOH solutions were used in each of the cells, as shown in Figure3.4. The total charges passing by (Q) was then calculated after six-hours via the following equation:

$$Q = \int I(t)\, d(t) \tag{3}$$

Where: Q is the total charges passing by, C. I is the current, mA, and t is the time, s.

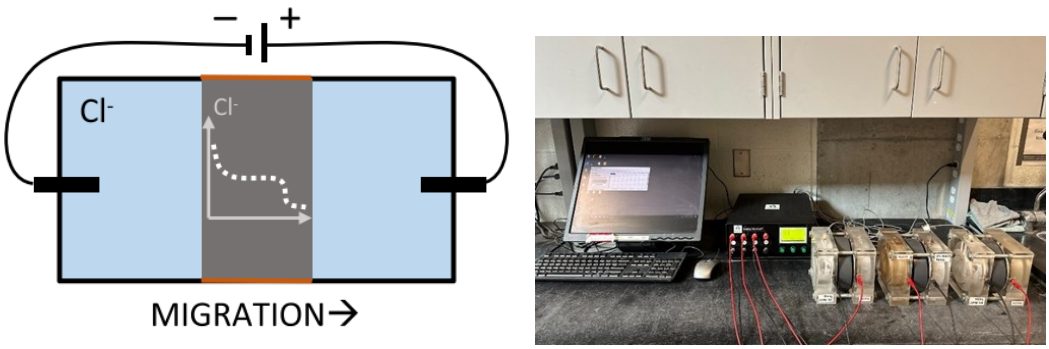

Figure 3.4. RCPT: (a) Schematic [13] and (b) Experiments in the laboratory.

3.5.7 Bulk diffusion test

3.5.7.1 Sample preparation and chloride content determination

The chloride bulk diffusion test was performed as per ASTM C1556 [16]. Following a 56-day curing period, all concrete specimens were cut into cylinders measuring 100 mm in diameter and 75 mm in length. To ensure unidirectional chloride diffusion, the cylindrical sides and bottom surfaces were sealed with epoxy resin, leaving only the top surface exposed. After allowing the epoxy to cure for 24 hours, specimens were submerged in a saturated calcium hydroxide solution for at least 24 additional hours to establish chemical equilibrium. Mass stability was then verified by confirming that the mass variation remained within ±0.1%. Once this condition was met, all specimens were immersed in a 165 g/L sodium chloride (NaCl) solution to begin the diffusion test, as illustrated in Fig 3.5. After 90 days of exposure, the specimens were removed and prepared for chloride profiling. Chloride profiles were obtained by sequentially grinding the exposed surface in depth increments of 1–3 mm. The collected powders were oven-dried at 105 °C to a constant mass and then sieved through a 600 µm mesh to obtain homogeneous samples. The total chloride content was determined by potentiometric titration of dissolving the powder into acid-based, followed by ASTM C1152 [47].

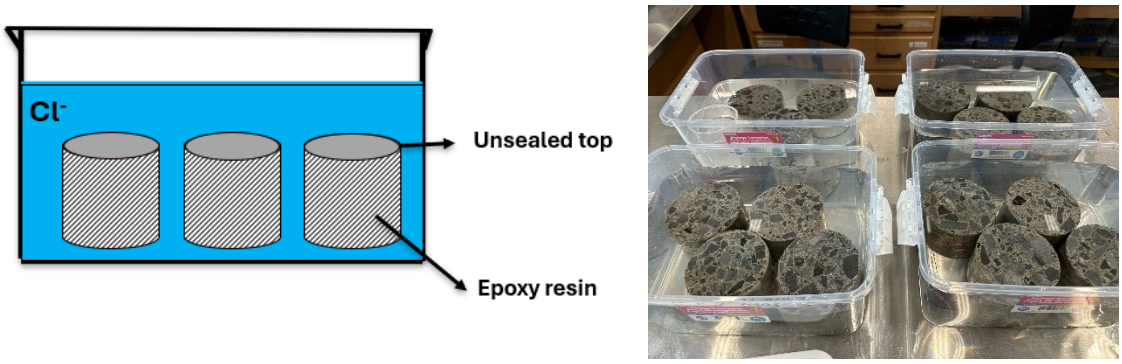

(a) (b)

Figure 3.5. Bulk diffusion test: (a) Schematic and (b) Experiments in the laboratory.

3.5.7.2 Apparent diffusion coefficient (Da)

After determining the total chloride content (expressed as a mass percentage of concrete) at each depth, the chloride concentration profile was constructed. Based on this profile, the apparent chloride diffusion coefficient (Da) is calculated using Fick's Second Law of Diffusion, as defined by the following equation:

$$C(xt) = Cs \cdot (1 - erfc\left(\frac{x}{2\sqrt{Dat}}\right)) \quad (4)$$

Where: C(xt) is the chloride content in depth x and after time t, mass % of concrete, Cs is the estimated surface chloride content, mass % of concrete, Da is the apparent diffusion coefficient, $\times 10^{-12}$ m^2/s, erfc is the error function, given in standard mathematic book.

It was worth mentioning that Cs does not represent a physically measurable value, but is rather a fitting parameter used solely for computational purposes within the diffusion model [15].

Figure 3.6. illustrates the overall sequence of curing and testing procedures. It is important to note that, due to the specific size requirements of the RCPT and bulk diffusion test that the electrical resistivity measurements (including bulk ER and surface ER) were conducted first. Within the following 24 hours, the RCPT and the initiation of the bulk diffusion test were performed. To ensure consistency and enable direct comparison across different test methods, all evaluations were performed on the same set of specimens for each mixture, and an identical curing period was maintained throughout the testing program.

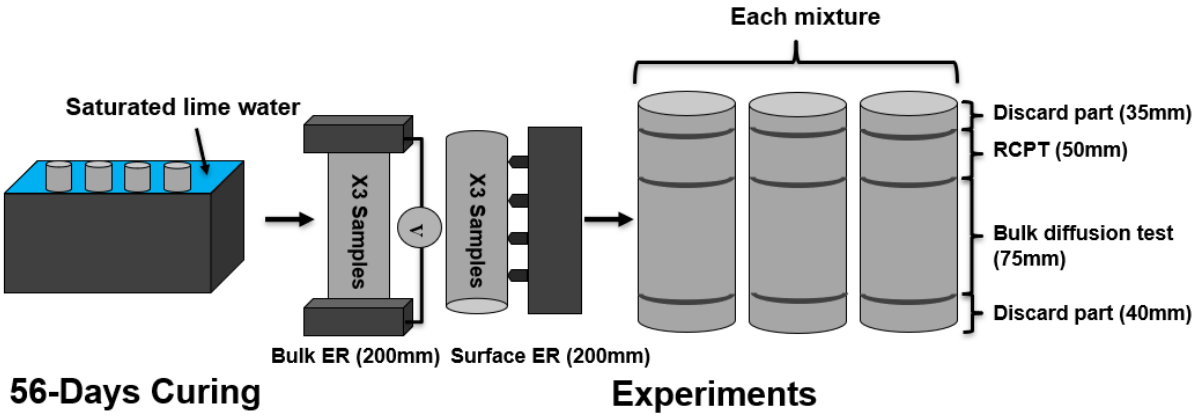

Figure 3.6. Schematic of sample preparation and testing.

3.6 Results

3.6.1 Electrical accelerated test

Figure 7 and Figure 8 present the bulk ER, surface ER and RCPT results for the 15 PLC concrete mixtures incorporating PLC with varying proportions of fly ash and slag. The red lines “Low”, “Very low,” et al. shown in the figures represent the chloride penetrability in concrete in accordance with Table 3.1.

3.6.1.1 Electrical resistivity test

Figure 3.7(a) illustrates the Bulk ER values across various mixture designs. As anticipated, the incorporation of SCMs, such as fly ash and slag, significantly enhanced the electrical resistivity of the concrete. Mixtures such as AS40, H1S20, and H2S40 demonstrated the highest Bulk ER values, all exceeding 200 Ω·m, which corresponds to the classification of very low chloride ion penetrability. In contrast, the pure PLC mixtures, A, H1, and H2, exhibited substantially lower Bulk ER values, all below 100 Ω·m, indicating moderate chloride penetrability. Mixtures incorporating moderate SCM contents (i.e., 20%) generally ranged between 100 and 200 Ω·m, placing them within the low chloride penetrability category.

Figure 3.7(b) presents the surface electrical resistivity (Surface ER) values, which follow a similar trend to the Bulk ER results. The mixtures with 40% slag addition, particularly AS40, H1S20, and H2S40, achieved the highest surface resistivity values, all exceeding 37 kΩ·cm, classifying them within the very low chloride penetrability range. Conversely, the pure PLC mixtures again showed the lowest resistivity values, consistently below 15 kΩ·cm, corresponding to moderate chloride ion penetrability.

(a)

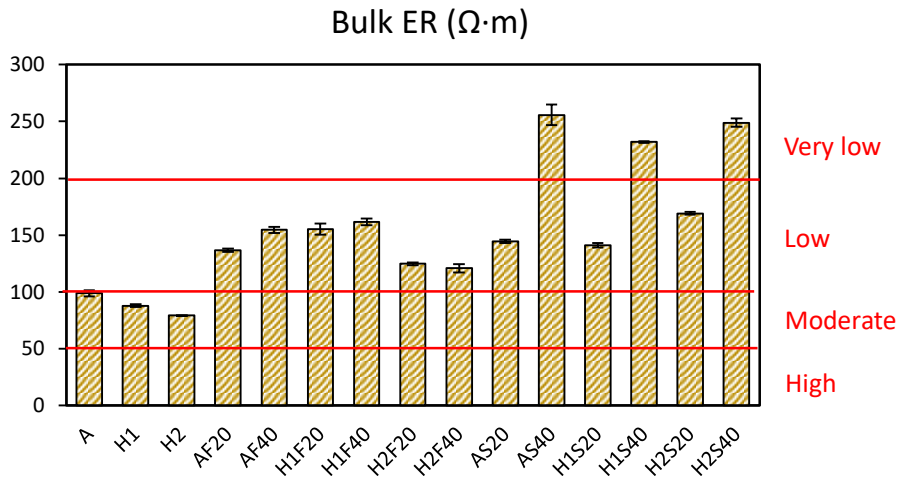

(b)

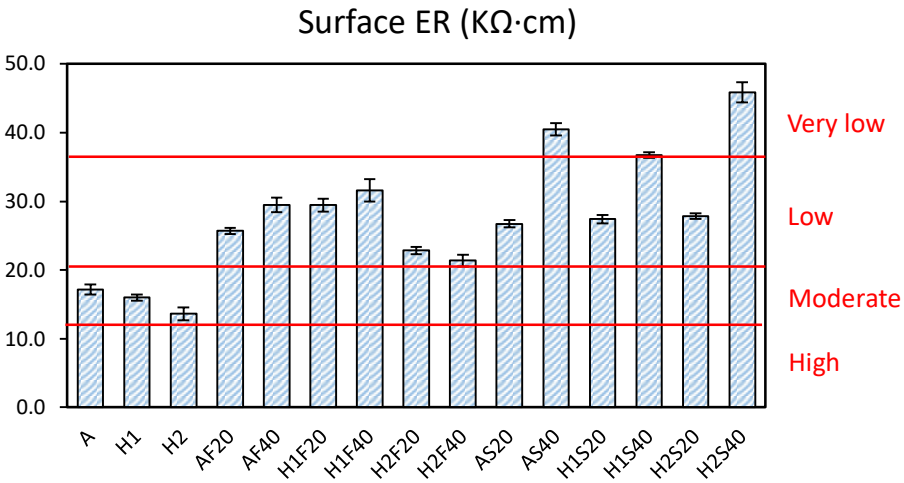

Figure 3.7. Electrical resistivity test results: (a) Bulk ER and (b) Surface ER at 56 days.

3.6.1.2 RCPT

Figure 3.8. presents the results of the RCPT, expressed in terms of total charge passed (coulombs, C). The RCPT outcomes reveal distinct trends in chloride resistance, closely correlated with the type and proportion of SCMs incorporated. Mixtures containing slag, specifically AS20, AS40,

H1S40, and H2S40, demonstrated significantly reduced charge values, all below 1000 C, placing them within the very low chloride permeability category according to ASTM C1202 classifications.

In contrast, mixtures incorporating fly ash and the pure PLC systems (i.e., A, H1, and H2) exhibited higher total charges, indicative of comparatively greater ionic mobility. These mixtures generally fell within the low chloride permeability range. The results underscore the superior performance of slag-blended systems in mitigating chloride ingress and support the observed trends from resistivity testing, further highlighting the beneficial role of high slag content in enhancing chloride resistance in PLC concretes.

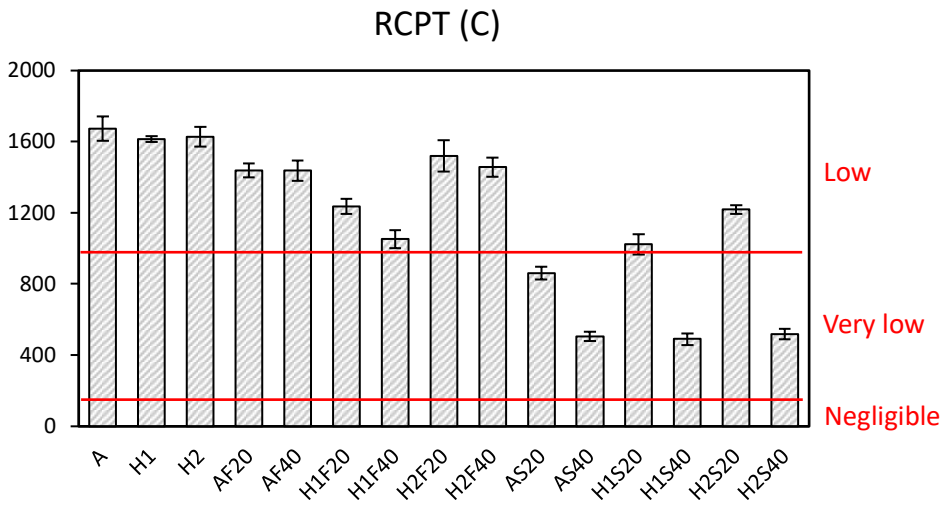

Figure 3.8. RCPT results at 56 days.

Furthermore, with the incorporation of fly ash, the results from Bulk ER, Surface ER, and RCPT consistently demonstrate an improvement in chloride resistance as the limestone replacement level increases from A to H1. This enhancement may be attributed to the synergistic effect between fly ash and a moderate amount of limestone filler, which promotes the formation of additional hydration products and contributes to microstructural densification [28]. However, when the limestone replacement level is further increased to H2, this synergistic benefit appears to diminish. At this point, the dilution effect becomes more pronounced, where the reduced clinker content leads to a decrease in overall hydration product formation, and ultimately resulting in a decline in chloride

resistance. This observation suggests that there exists an optimal limestone replacement threshold beyond which the beneficial interactions with fly ash are no longer sufficient to offset the negative impact on chloride resistance.

3.6.2 Bulk diffusion test

3.6.2.1 Chloride profile

The chloride profiles after 90 days of bulk diffusion testing by following ASTM C1556 are shown in Figure 3.9. For the following Da calculation simplicity, all the chloride content is noted as mass % of dry concrete powder.

Without SCMs, the chloride content consistently decreased with increasing depth across all cement types (A, H1, and H2), reflecting the typical diffusion-driven ingress behavior. When incorporated with fly ash, a clear improvement in chloride resistance was noted. Increasing fly ash content from 20% (i.e., AF20, H1F20, H2F20) to 40% (i.e., AF40, H1F40, H2F40) significantly reduced chloride ingress at all depths. This phenomenon was amplified with the addition of slag. Mixtures containing 40% slag (i.e., AS40, H1S40, H2S40) exhibited notably lower chloride ingress compared to those with only 20% slag (AS20, H1S20, H2S20), demonstrating the effectiveness of slag in reducing chloride diffusion. The chloride content at depths greater than 5 mm was considerably lower in the slag mixtures compared to pure and fly ash addition mixtures.

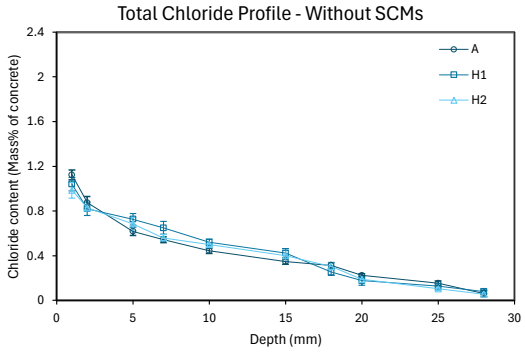

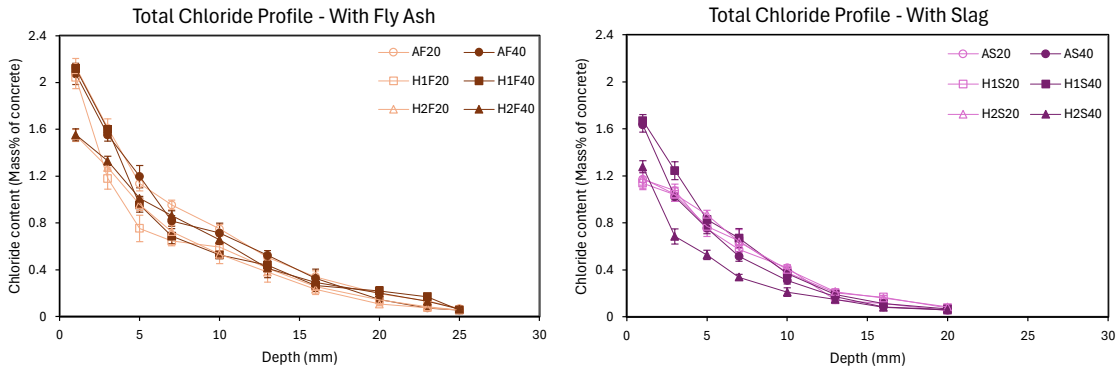

Figure 3.9. Chloride profiles.

3.6.2.2 Apparent diffusion coefficient (Da)

After all of the chloride profiles were analysed, Da could be computed by Eq (1) in accordance with Fick's second law. Figure 3.10. illustrates the Da of different mixtures. In pure PLC mixtures, Da increased when limestone content increased from A to H1, reaching a peak at H2 mixture limestone replacement, which achieves 16.82 × 10^{-12}×m^2/s of three samples average. The incorporation of fly ash reduced the chloride diffusion coefficients across all limestone replacement levels except H2F40, which may be influenced by the dilution effect of limestone filler. Similarly, slag inclusion significantly enhanced chloride resistance. Mixtures with slag consistently exhibited reduced Da compared to pure PLC mixtures. Among all mixtures, H2S40 recorded the lowest Da value, which reaches 2.63 × 10^{-12}×m^2/s by average values.

It deserves to be mentioned that fly ash and slag demonstrate different effects and are shown in electrical accelerated test and Da results, The increase of fly ash content from 20% to 40% did not display quite largely influenced the two mixtures, for instance, AF20 and AF40 presented similar values in each test. However, with the addition of slag, increased slag content from 20% to 40% clearly demonstrated benefits in chloride resistance.

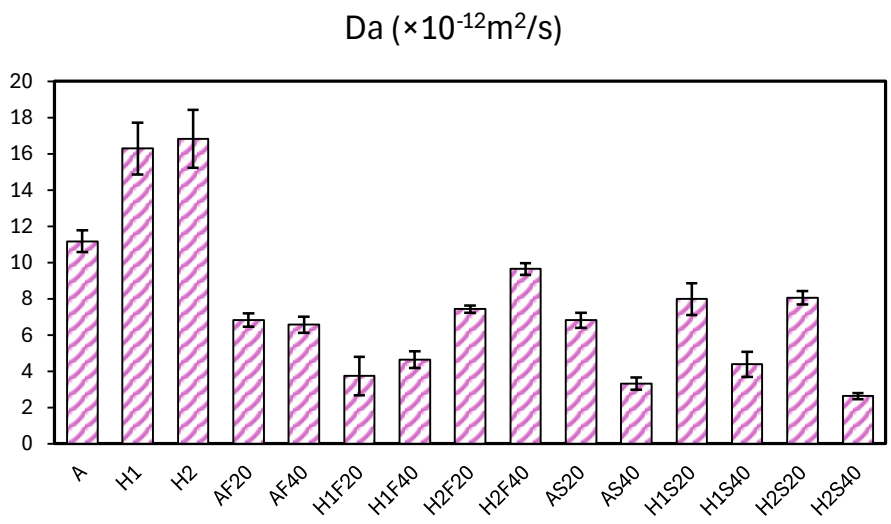

Figure 3.10. Apparent diffusion coefficient (Da) in different PLC mixtures.

3.7 Discussion

3.7.1 Da validation

Bulk diffusion test is considered the most reliable method to reflect chloride resistance since its natural diffusion process. To assess chloride resistance accurately among all of the concrete mixtures, the one-way analysis of variance (ANOVA) with a confidence level of 95 % was conducted first to confirm the significance of Da on different mixtures (i.e., PLC, PLC + Fly ash, and PLC + Slag), as shown in Table 3.4. The F-value represents the ratio of variance between groups to the variance within groups. A higher F-value indicates a greater likelihood that observed differences are not due to random variation. To assess significance, the calculated F-value is compared to the Fcritical value (noted Fcrit), which is determined based on the seleted significance level (commonly $\alpha = 0.05$) and the degrees of freedom associated with the test. If the F-value exceeds the Fcrit, the null hypothesis, stating that all group means are equal, is rejected, indicating a statistically significant difference among groups. Additionally, the p-value provides a probabilistic measure of the likelihood that the observed differences occurred by chance. A p-value less than 0.05 is typically considered statistically significant, confirming the result indicated by the

F-test. In summary, a statistically significant outcome is confirmed when F > Fcrit and p < 0.05, implying that at least one group mean differs meaningfully from the others.

Table 3.4. One-way ANOVA on Da.

Test name	**F**	**F_{crit}**	**P**	**Significant**
Pure PLC	17.62	5.14	0.003	✓
PLC + Fly ash	43.02	3.11	2.98E-07	✓
PLC + Slag	61.45	3.11	3.94E-08	✓

3.7.1.1 Pure PLC mixtures

When a one-way ANOVA indicates statistically significant differences among group means, Tukey's honestly significant difference (HSD) post hoc test is applied to identify which specific pairs of groups differ. In practical terms, for each pair of mixtures, the factor level line that does not include zero confirms that the difference is statistically significant. The pure PLC mixture's detailed comparison is shown in Figure 3.11.

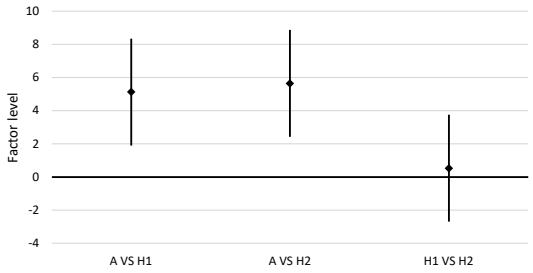

Figure 3.11. Tukey test of pure PLC mixtures.

Based on the results of the statistical analysis, the results of mixture A are significantly different from mixtures H1 and H2. However, this should not be interpreted as definitive evidence that increasing interground limestone content necessarily reduces chloride resistance. As previously discussed, at a constant W/P ratio higher limestone replacement provides less hydration products which in turn generates less densified microstructure. To further investigate this aspect, Fig 3.12. illustrates the relationship among the Da, W/P ratio and the water-to-clinker ratio in pure PLC mixtures.

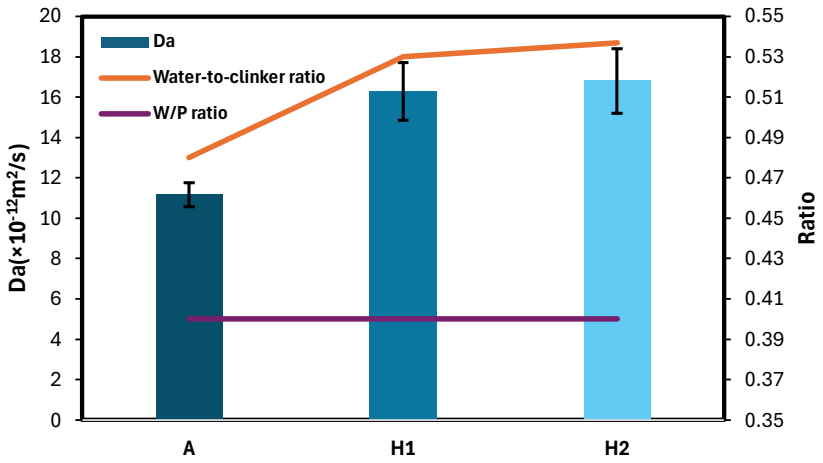

Figure 3.12. The relationship of Da, W/P ratio and water-to-clinker ratio.

The figure above shows that changes in Da closely follow the trend of the water-to-clinker ratio, suggesting that this parameter serves as a more accurate indicator of chloride resistance performance than W/P ratio. In PLC systems, a lower water-to-clinker ratio promotes more complete hydration, resulting in a denser microstructure and improved chloride resistance. This finding indirectly supports the feasibility of using high-limestone PLC in future applications. By optimizing concrete mix design to better control the water-to-clinker ratio, it is possible to maintain or even enhance durability performance. Thus, even in systems with elevated limestone content, PLC can still be effectively employed, reinforcing its potential as a sustainable alternative in low-carbon construction.

3.7.1.2 Binary blended PLC with SCMs

Following the analysis of the pure PLC mixtures, it is evident that different SCMs contribute to distinct enhancing chloride resistance. The detailed analysis of these effect is presented in Fig 3.13.

a)

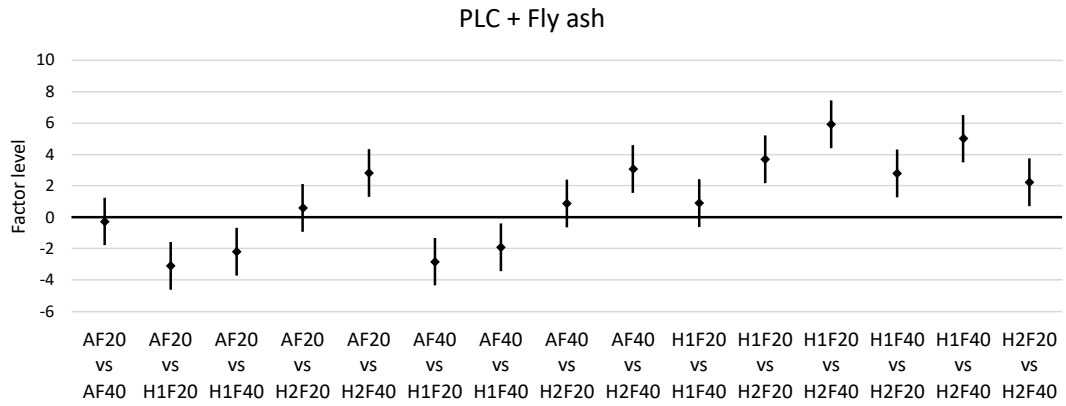

b)

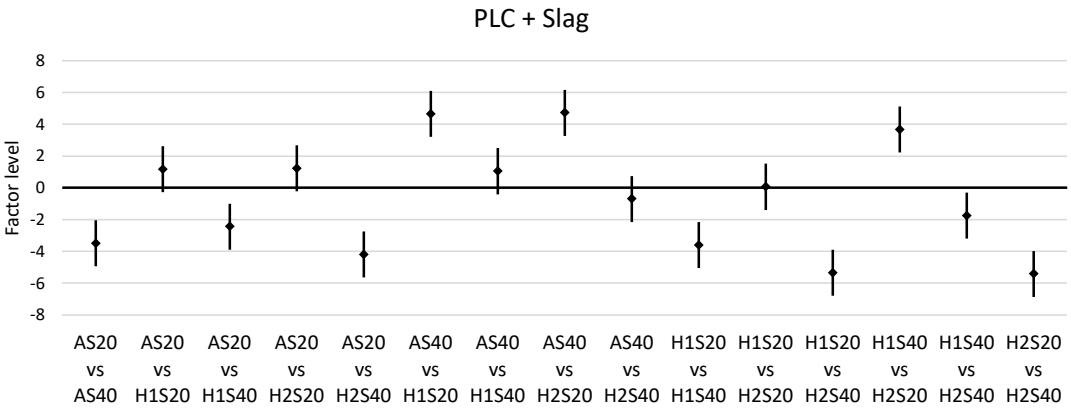

Figure 3.13. Tukey test on blended PLC mixtures.

Based on the results of the Tukey post-hoc test, the chloride resistance performance of various PLC mixtures was statistically compared. The significant difference observed between H1S40 and H2S40 may be attributed to the relatively low variance or error margin associated with the H2S40 data. As anticipated, the influence of SCMs incorporation on chloride resistance varied depending on the level of interground limestone replacement. The interaction between limestone content and SCM type (i.e., fly ash or slag) exhibited distinct trends in enhancing chloride resistance across different mixtures. The underlying reason likely stems from the fact that slag, unlike fly ash, does not heavily depend on the hydration products generated by PLC to trigger the formation of secondary hydration products. As a result, the overall enhancement in chloride resistance becomes

more pronounced when increasing slag content from 20% to 40%. In contrast, for the fly ash blended mixtures, background research suggests that fly ash reacts with interground limestone to form additional carboaluminate phases. Among the six fly ash mixtures evaluated, the H1 limestone replacement appears to optimize chloride resistance, likely due to the favorable hydration kinetics.

3.7.2 The correlation of Da & Resistivity tests

As previously discussed, Da serves as a key indicator of overall chloride resistance. In this context, the relationship between Da and various accelerated testing methods, such as electrical resistivity tests and the RCPT, becomes particularly relevant. Figure 3.14 illustrates the correlation between Da and resistivity measurements. In the figure, darker-colored markers represent the average values derived from three specimens for each mixture.

The results reveal a strong correlation between Da and both bulk ER and surface ER, reinforcing the connection between resistivity and chloride resistance. Given that resistivity testing reflects the pore structure of concrete, this correlation underscores the critical role of microstructure in influencing chloride resistance. Mixtures incorporating SCMs consistently exhibit lower Da values and higher resistivity, indicating the beneficial effect of SCMs in refining the concrete microstructure.

Interestingly, while mixtures with fly ash and slag additions show comparable Da values, the slag containing mixtures demonstrate notably higher resistivity. This discrepancy is likely attributed to differences in the ionic strength of the pore solution introduced by the two SCM types. The lower ionic conductivity in slag-blended systems contributes to higher resistivity readings despite similar levels of chloride resistance.

a)

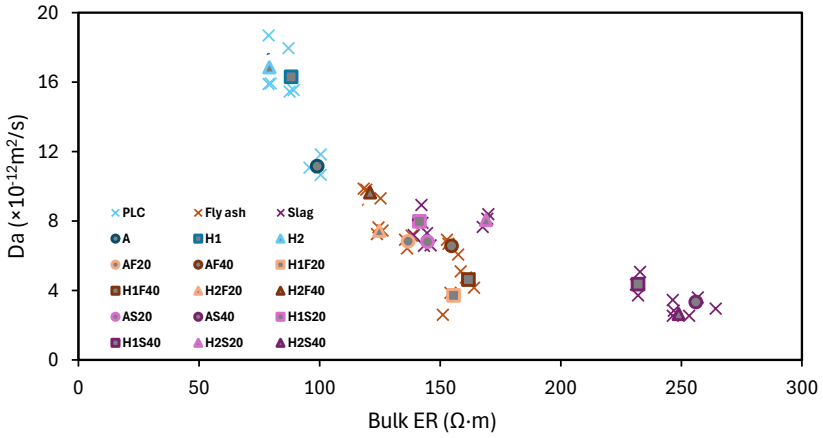

b)

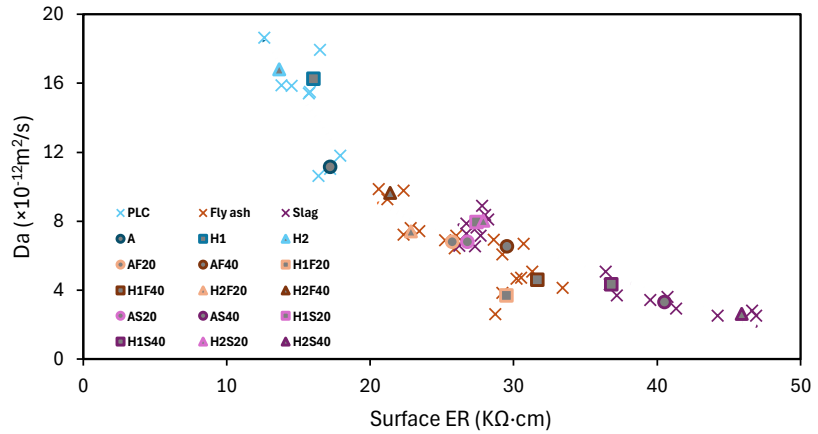

Figure 3.14. The correlation of Da and resistivity test: (a) Da vs bulk ER and (b) Da vs surface ER.

3.7.3 The correlation of Da & RCPT

Similar to resistivity testing, RCPT serves as another accelerated method, and its correlation with Da further highlights its practical relevance. Fig 3.15. presents the relationship between Da and RCPT results across all PLC mixtures. As shown in the figure, mixtures incorporating SCMs exhibit a strong correlation between reduced charge passed and lower Da values, indicating enhanced chloride resistance.

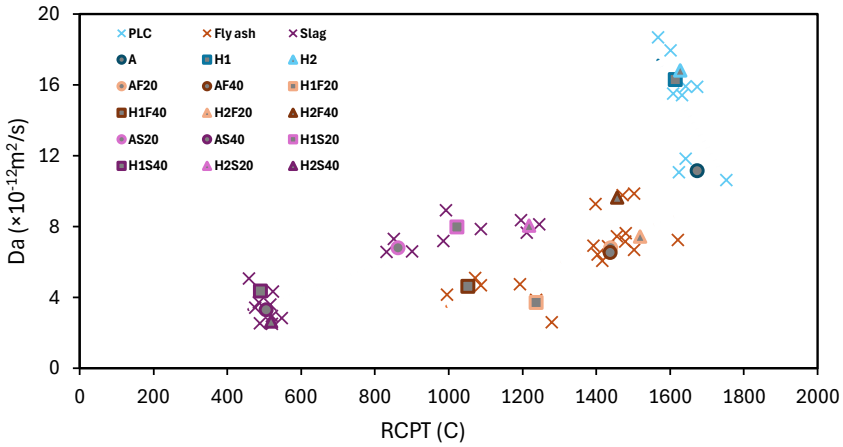

Figure 3.15. The correlation of Da and RCPT.

However, for the pure PLC mixtures, a discrepancy is observed. While the Da values indicate clear differences in chloride resistance among A, H1, and H2, the RCPT results do not reflect similarly significant variation. To further investigate this inconsistency, a one-way ANOVA, which similar to the analysis described in Section 3.7.1, was conducted to assess whether each accelerated method (Bulk ER, Surface ER, and RCPT) can effectively differentiate chloride resistance performance among all mixtures. This statistical evaluation provides insight into the discriminatory capability of each test and helps determine their respective reliability in capturing meaningful differences in chloride resistance.

Table 3.5 One-way ANOVA of acceleration tools.

Test name	**F**	**F_{crit}**	**P**	**Significant**
			Bulk ER	
Pure PLC	101.62	5.14	2.36E-05	✓
PLC + Fly ash	97.79	3.11	2.69E-09	✓
PLC + Slag	501.47	3.11	1.70E-13	✓
			Surface ER	
Pure PLC	17.40	5.14	0.003	✓
PLC + Fly ash	51.27	3.11	1.11E-07	✓
PLC + Slag	289.84	3.11	4.45E-12	✓
			RCPT	
Pure PLC	1.05	5.14	0.41	X
PLC + Fly ash	28.42	3.11	2.95E-06	✓
PLC + Slag	228.22	3.11	1.80E-11	✓

From Table 3.5, the ANOVA results confirm that all three accelerated testing methods are generally reliable in capturing meaningful differences in chloride resistance among the various mixtures. However, consistent with previous observations, RCPT failed to identify statistically significant differences among the pure PLC mixtures. Similar findings have also been reported in prior literature, suggesting a potential limitation of the RCPT method under certain conditions [43].

One plausible explanation lies in the inherent characteristics of the RCPT procedure. The test involves applying a constant 60 V voltage across the specimen for six hours, which can result in temperature increases within the testing cell. This effect tends to be more pronounced in mixtures with lower electrical resistivity values, such as the pure PLC systems examined in this study. The elevated temperature accelerates ionic movement, leading to higher charge passage through these lower-resistivity specimens. As a result, the RCPT may underestimate differences in chloride resistance between similar mixtures, thereby masking subtle but meaningful variations that are otherwise captured by Da or resistivity tests.

3.8 Conclusion

This study investigates the chloride resistance performance of PLC concrete incorporating various types and levels of supplementary cementitious materials (SCMs) using multiple evaluation methods. The main findings are summarized as follows:

- Based on the chemical composition analysis of the three interground limestone cements (A, H1, and H2), certain values observed in H1 and H2 were unexpected, particularly given their higher limestone replacement levels. These anomalies highlight the influence of the cement manufacturing process on final chemical composition, particularly in high-limestone PLCs. Therefore, it is essential to implement tighter production control and optimized quality assurance protocols to ensure consistency in performance and facilitate the broader adoption of sustainable PLC systems.

- Results from this study indicate that the water-to-clinker ratio, as opposed to the water-to-powder (W/P) ratio, is a more suitable parameter for characterizing the relationship with chloride resistance, particularly in high interground limestone systems (above 15% replacement, as examined in this study). This finding provides important insights into optimizing mixture design and highlights the potential for further increasing limestone replacement levels while still achieving satisfactory long-term durability performance.

- The quite good correlation observed between Bulk ER, Surface ER, and the apparent diffusion coefficient (Da) confirms that pore structure plays a critical role in determining chloride resistance in PLC systems. Mixtures exhibiting denser microstructures consistently show lower Da values, indicating enhanced resistance to chloride ingress. These findings underscore the importance of microstructural refinement, achieved through optimized binder composition and SCM incorporation, in improving the durability performance of PLC-based concretes.

- The rapid chloride permeability test (RCPT) was unable to distinguish differences in chloride resistance among pure PLC mixtures, as confirmed through statistical analysis. This finding underscores the need for future optimization of RCPT and similar accelerated test methods, particularly to improve their sensitivity and reliability in evaluating low-resistivity concrete systems such as pure PLC systems.

3.9 References

[1] C. R. Gagg, "Cement and concrete as an engineering material: An historic appraisal and case study analysis," *Eng. Fail. Anal.*, vol. 40, pp. 114–140, May 2014, doi: 10.1016/j.engfailanal.2014.02.004.

[2] "4 ways to make the cement industry more sustainable," World Economic Forum. Accessed: Apr. 05, 2025.

[3] I. Al Khaffaf, R. A. Hawileh, S. Sahoo, J. A. Abdalla, and J. H. Kim, "Toward carbon-neutral construction: A review of zero-carbon concrete," *J. Build. Eng.*, vol. 99, p. 111578, Apr. 2025, doi: 10.1016/j.jobe.2024.111578.

[4] S. B. Nia, A. Nyland, J. Wivast, M. Kioumarsi, and B. Shafei, “Investigations of portland limestone cement and waste glass powder for sustainable ultra-high performance concrete,” *Case Stud. Constr. Mater.*, vol. 22, p. e04425, Jul. 2025, doi: 10.1016/j.cscm.2025.e04425.

[5] J. Lee, B. Lothenbach, and J. Moon, “Performance improvement of Portland-limestone cement by mechanochemical activation,” *Cem. Concr. Res.*, vol. 176, p. 107411, Feb. 2024, doi: 10.1016/j.cemconres.2023.107411.

[6] K.-H. Yang, Y.-B. Jung, M.-S. Cho, and S.-H. Tae, “Effect of supplementary cementitious materials on reduction of CO2 emissions from concrete,” *J. Clean. Prod.*, vol. 103, pp. 774–783, Sep. 2015, doi: 10.1016/j.jclepro.2014.03.018.

[7] K. A. Knight, P. R. Cunningham, and S. A. Miller, “Optimizing supplementary cementitious material replacement to minimize the environmental impacts of concrete,” *Cem. Concr. Compos.*, vol. 139, p. 105049, May 2023, doi: 10.1016/j.cemconcomp.2023.105049.

[8] A. Ahmed, “Assessing the effects of supplementary cementitious materials on concrete properties:a review,” *Discov. Civ. Eng.*, vol. 1, no. 1, pp. 1–47, Dec. 2024, doi: 10.1007/s44290-024-00154-z.

[9] V. V. Sai Chand, B. Kameswara Rao, and Ch. Hanumantha Rao, “Investigation on chloride penetration in concrete mixes of different cement replacement percentages with fly ash and silica fume,” *Mater. Today Proc.*, vol. 33, pp. 820–827, Jan. 2020, doi: 10.1016/j.matpr.2020.06.270.

[10] L. Tong, B. Šavija, M. Zhang, Q. X. Xiong, and Q. Liu, “Chloride penetration in concrete under varying humidity and temperature changes: A numerical study,” *Constr. Build. Mater.*, vol. 458, p. 138380, Jan. 2025, doi: 10.1016/j.conbuildmat.2024.138380.

[11] R. Loser, B. Lothenbach, A. Leemann, and M. Tuchschmid, “Chloride resistance of concrete and its binding capacity – Comparison between experimental results and thermodynamic modeling,” *Cem. Concr. Compos.*, vol. 32, no. 1, pp. 34–42, Jan. 2010, doi: 10.1016/j.cemconcomp.2009.08.001.

[12] M. T. E. Amin, P. K. Sarker, F. U. A. Shaikh, and A. Hosan, “Chloride permeability and chloride-induced corrosion of concrete containing lithium slag as a supplementary cementitious material,” *Constr. Build. Mater.*, vol. 471, p. 140629, Apr. 2025, doi: 10.1016/j.conbuildmat.2025.140629.

[13] W. Wilson, F. Georget, and K. Scrivener, “Unravelling chloride transport/microstructure relationships for blended-cement pastes with the mini-migration method,” *Cem. Concr. Res.*, vol. 140, p. 106264, Feb. 2021, doi: 10.1016/j.cemconres.2020.106264.

[14] B. Martín-Pérez, H. Zibara, R. D. Hooton, and M. D. A. Thomas, “A study of the effect of chloride binding on service life predictions,” *Cem. Concr. Res.*, vol. 30, no. 8, pp. 1215–1223, Aug. 2000, doi: 10.1016/S0008-8846(00)00339-2.

[15] K. De Weerdt, W. Wilson, A. Machner, and F. Georget, “Chloride profiles – What do they tell us and how should they be used?,” *Cem. Concr. Res.*, vol. 173, p. 107287, Nov. 2023, doi: 10.1016/j.cemconres.2023.107287.

[16] ASTM C1556-22 Standard Test Method for Determining the Apparent Chloride Diffusion Coefficient of Cementitious Mixtures by Bulk Diffusion, ASTM International, 2022.

[17] Canada - CSA A23.1:24/CSA A23.2:24 Concrete materials and methods of concrete construction/Test Methods and Standard Practices for concrete - NimonikApp.com.” Accessed: Apr. 05, 2025.

[18] AASHTO TP 95 - Standard Method of Test for Surface Resistivity Indication of Concrete’s Ability to Resist Chloride Ion Penetration | GlobalSpec.” Accessed: Apr. 01, 2024.

[19] ASTM C1202 Standard Test Method for Electrical Indication of Concrete’s Ability to Resist Chloride Ion Penetration.

[20] Portland Cement Association *et al.*, “State-of-the-Art Report on Use of Limestone in Cements at Levels of up to 15%,” Portland Cement Association, 2024. doi: 10.70909/pca.2024.SN3148.03.

[21] K. Bharadwaj *et al.*, “CALTRANS: Impact of the Use of Portland-Limestone Cement on Concrete Performance as Plain or Reinforced Material,” Kiewit Center, Nov. 2021. doi: 10.5399/osu/1150.

[22] “Sustainable construction for a circular economy,” Cement Association of Canada. Accessed: Apr. 06, 2025. [Online]. Available: https://cement.ca/sustainability/portland-limestone-cement/

[23] D. Wang, C. Shi, N. Farzadnia, Z. Shi, H. Jia, and Z. Ou, “A review on use of limestone powder in cement-based materials: Mechanism, hydration and microstructures,” *Constr. Build. Mater.*, vol. 181, pp. 659–672, Aug. 2018, doi: 10.1016/j.conbuildmat.2018.06.075.

[24] Y. Briki, M. Zajac, M. B. Haha, and K. Scrivener, “Impact of limestone fineness on cement hydration at early age,” *Cem. Concr. Res.*, vol. 147, p. 106515, Sep. 2021, doi: 10.1016/j.cemconres.2021.106515.

[25] A. C. Bergmann *et al.*, “Influence of Interparticle Separation Distance on the Fresh and Hardened Behavior of Ecoefficient Cement Pastes,” *J. Mater. Civ. Eng.*, vol. 35, no. 8, p. 04023252, Aug. 2023, doi: 10.1061/JMCEE7.MTENG-14988.

[26] G. Kakali, S. Tsivilis, E. Aggeli, and M. Bati, “Hydration products of C3A, C3S and Portland cement in the presence of CaCO3,” *Cem. Concr. Res.*, vol. 30, no. 7, pp. 1073–1077, Jul. 2000, doi: 10.1016/S0008-8846(00)00292-1.

[27] G. Menéndez, V. Bonavetti, and E. F. Irassar, “Strength development of ternary blended cement with limestone filler and blast-furnace slag,” *Cem. Concr. Compos.*, vol. 25, no. 1, pp. 61–67, Jan. 2003, doi: 10.1016/S0958-9465(01)00056-7.

[28] K. De Weerdt, K. O. Kjellsen, E. Sellevold, and H. Justnes, “Synergy between fly ash and limestone powder in ternary cements,” *Cem. Concr. Compos.*, vol. 33, no. 1, pp. 30–38, Jan. 2011, doi: 10.1016/j.cemconcomp.2010.09.006.

[29] K. De Weerdt, “Chloride binding in concrete: recent investigations and recognised knowledge gaps: RILEM Robert L’Hermite Medal Paper 2021,” *Mater. Struct.*, vol. 54, no. 6, pp. 1–16, Dec. 2021, doi: 10.1617/s11527-021-01793-9.

[30] C. Li and L. Jiang, “The role of chloride binding mechanism in the interpretation of chloride profiles in concrete containing limestone powder,” *J. Sustain. Cem.-Based Mater.*, vol. 12, no. 1, pp. 24–35, Jan. 2023, doi: 10.1080/21650373.2021.2010243.

[31] B. Lothenbach, K. Scrivener, and R. D. Hooton, “Supplementary cementitious materials,” *Cem. Concr. Res.*, vol. 41, no. 12, pp. 1244–1256, Dec. 2011, doi: 10.1016/j.cemconres.2010.12.001.

[32] M. T. De Grazia, H. Deda, and L. F.M. Sanchez, “The influence of the binder type & aggregate nature on the electrical resistivity of conventional concrete,” *J. Build. Eng.*, vol. 43, p. 102540, Nov. 2021, doi: 10.1016/j.jobe.2021.102540.

[33] H. Yildirim, T. Ilica, and O. Sengul, “Effect of cement type on the resistance of concrete against chloride penetration,” *Constr. Build. Mater.*, vol. 25, no. 3, pp. 1282–1288, Mar. 2011, doi: 10.1016/j.conbuildmat.2010.09.023.

[34] D. G. Mapa, H. Zhu, F. Nosouhian, N. Shanahan, K. A. Riding, and A. Zayed, “Chloride binding and diffusion of slag blended concrete mixtures,” *Constr. Build. Mater.*, vol. 388, p. 131584, Jul. 2023, doi: 10.1016/j.conbuildmat.2023.131584.

[35] A. Runci, J. Provis, and M. Serdar, “Microstructure as a key parameter for understanding chloride ingress in alkali-activated mortars,” *Cem. Concr. Compos.*, vol. 134, p. 104818, Nov. 2022, doi: 10.1016/j.cemconcomp.2022.104818.

[36] R. Taylor, I. G. Richardson, and R. M. D. Brydson, “Composition and microstructure of 20-year-old ordinary Portland cement–ground granulated blast-furnace slag blends containing 0 to 100% slag,” *Cem. Concr. Res.*, vol. 40, no. 7, pp. 971–983, Jul. 2010, doi: 10.1016/j.cemconres.2010.02.012.

[37] K. A. Snyder, P. E. Stutzman, J. Philip, and D. Esh, “HYDRATED PHASES IN BLENDED CEMENTITIOUS SYSTEMS FOR NUCLEAR INFRASTRUCTURE”.

[38] Z. Xu and G. Ye, “Understanding Chloride Diffusion Coefficient in Cementitious Materials,” *Materials*, vol. 16, no. 9, Art. no. 9, Jan. 2023, doi: 10.3390/ma16093464.

[39] M. Thomas and T. Bremner, “Performance of lightweight aggregate concrete containing slag after 25years in a harsh marine environment,” *Cem. Concr. Res.*, vol. 42, no. 2, pp. 358–364, Feb. 2012, doi: 10.1016/j.cemconres.2011.10.009.

[40] M. Bonta, A. Eitzenberger, S. Burtscher, and A. Limbeck, “Quantification of chloride in concrete samples using LA-ICP-MS,” *Cem. Concr. Res.*, vol. 86, pp. 78–84, Aug. 2016, doi: 10.1016/j.cemconres.2016.05.002.

[41] W. Wilson, F. Georget, and K. L. Scrivener, “XCr/√t as an Indicator of the Resistance Against Bulk Chloride Diffusion,” in *International RILEM Conference on Synergising Expertise towards Sustainability and Robustness of Cement-based Materials and Concrete Structures*, Springer, Cham, 2023, pp. 658–666. doi: 10.1007/978-3-031-33211-1_59.

[42] Correlation Between Bulk and Surface Resistivity of Concrete,” *ResearchGate*, Oct. 2024, doi: 10.1007/s40069-014-0094-z.

[43] Y. A. Villagrán-Zaccardi and C. Andrade, “Chloride ingress rate and threshold content, as determined by the ‘Integral’ test method, in concrete with several w/c ratios in saturated and unsaturated conditions,” *Dev. Built Environ.*, vol. 8, p. 100062, Sep. 2021, doi: 10.1016/j.dibe.2021.100062.

[44] CSA A23.1. Concrete materials and methods of concrete construction/Test Methods and Standard Practices for concrete.

[45] ASTM C1876-24 Standard Test Method for Bulk Electrical Resistivity or Bulk Conductivity of Concrete.

[46] I. Mariani, “Evaluating Concrete Quality with Electrical Resistivity Test,” Giatec Scientific Inc. Accessed: Apr. 07, 2025. https://www.giatecscientific.com/education/evaluating-concrete-quality-with-electrical-resistivity/

[47] ASTM C1152/C1152M-20 Standard Test Method for Acid-Soluble Chloride in Mortar and Concrete, ASTM International, 2020.

Chapter 4

Investigation of Chloride Binding in High Interground Limestone Portland-Limestone Cement (PLC) Concrete

4.1 Abstract

Currently, concrete constitutes approximately 8% of global carbon dioxide emissions, with the majority of these emissions deriving from the manufacturing and use of Portland cement (PC). In light of concerns regarding global warming, proposed alternatives to decreasing carbon footprint include the use of interground limestone (Portland-limestone Cement [PLC]) and other supplementary cementitious materials (SCMs). As research on PLC concrete deepens, its long-term durability performance, particularly concerning chloride binding in delaying the ingress of chloride ions, has not been well understood. This paper presents the investigation of chloride binding of fifteen PLC concrete mixtures incorporating slag and fly ash with a fixed water-to-powder ratio (W/P) of 0.4. Different treatments (i.e., acid-soluble and water-soluble) of dry concrete powder were analyzed for chloride binding via automatic potentiometric titration. Results indicate that the chloride binding relationships are best described by the Langmuir isotherm, and it is found that the Al_2O_3/SO_3 ratio, rather than the singular Al_2O_3 content alone, provides a more accurate indicator of chloride binding capacity in pure PLC systems. As a result, this insight offers a promising pathway to maintain effective chloride binding even at high limestone replacement levels, provided that the cement manufacturing process is carefully controlled to optimize the sulfate-to-alumina balance. The incorporation of fly ash enhances chloride binding in binary blended PLC mixtures; however, varying levels of limestone replacement do not exhibit a significant impact on chloride binding with the addition of slag.

Keywords: Chloride binding, Portland-limestone cement (PLC), Supplementary cementitious materials (SCMs), Fly ash, Slag.

4.2 Introduction

Concrete is responsible for approximately 8% of global carbon dioxide (CO_2) emissions [1], with Portland cement (PC) being the primary contributor due to the carbon-intensive nature of its manufacturing process [2]. In response to this challenge, the Government of Canada has committed to a Net-Zero Emissions initiative [3], where 40% reduction should be achieved by 2030 whereas Net-Zero emissions are expected by 2050.

To address this shift, alternatives encompass the utilization of diverse categories of supplementary cementitious materials (SCMs), such as fly ash and slag, which are industrial by-products [4]. These materials can partially replace PC in concrete mixtures, thus decreasing partial clinker content and, consequently, reducing the CO_2 emissions. The other alternative method involves the replacement of interground limestone above 5% with clinker, the so-called Portland-limestone cement (PLC) [5]. In comparison to PC, the manufacturing of PLC markedly reduces CO_2 emissions and is completely authorized for usage in the United States, while being largely applied in construction projects in Canada [6]. As stated in the prevailing CSA A3000 standards [7], the maximum allowable limestone replacement in cement systems is set at 15%. Comprehensive research confirms that PLC with a 15% limestone replacement does not adversely affect the fresh-state, mechanical and durability-related properties of concrete when evaluated against the PC system [5,6,8].

However, moving forward to further reducing CO_2 emissions, the utilization of high interground limestone replacement, specifically above the current limestone limitation, as mentioned in CSA A3000, raises concerns regarding its long-term performance. One of the most harmful mechanisms impacting concrete durability worldwide is chloride-induced corrosion of reinforced concrete RC. External chloride ions, derived from de-icing salts and seawater ingress into the concrete, eventually reaching concrete rebars and initiating the corrosion process [9]. Chloride ions may chemically bind with cement hydration products (AFm) to form Cl-AFm, or more specifically,

Friedel's salt (Fs) solid solution. It can also physically bind with calcium aluminosilicate hydrates (C-A-S-H) within its diffuse layer [10,11]. In this context, the chloride binding capacity has emerged as a key factor in delaying the ingress of chloride ions into concrete, thereby extending the initiation period of corrosion. An elevated chloride binding corresponds to a reduced presence of "free" or mobile chloride ions in the concrete's pore solution, lowering the potential to trigger corrosion.

Existing studies preliminary focus on chloride binding in the PC systems [12-15]; however, there is a lack of data and understanding of chloride resistance in PLC concrete. This work evaluates the chloride binding capacity of PLC concrete mixtures incorporating distinct SCMs and amounts.

4.3 Background

4.3.1 Chloride composition in concrete

The total chloride content in concrete (expressed as a percentage of dry mass) is typically composed of three phases: chloride bound in Friedel's salt, chloride adsorbed in C-A-S-H, and free chloride ions dissolved in the pore solution. However, not all C-A-S-H phases contribute equally to chloride immobilization. De Weerdt et al. [10] identified that strongly bound chlorides, those considered immobile, are primarily stabilized within AFm interlayers (Cl-AFm) and are associated with approximately 10–20% of the C-A-S-H fraction. These strongly bound chlorides play a critical role in reducing chloride ingress and mitigating the risk of reinforcement corrosion [16]. This insight has significantly contributed to the understanding of chloride binding mechanisms and underscores the need for further research on the distinct roles of AFm and C-A-S-H phases in various cementitious systems, many of which remain insufficiently characterized.

Strongly bound chloride content in experimental studies can be estimated as the difference between acid-soluble and water-soluble chloride fractions [10]. This approach is based on the principle that both bound and free chloride ions dissolve completely in diluted nitric acid, while only the mobile

(free) chloride fraction is soluble in deionized [17] or distilled water [18]. Using potentiometric titration, chloride contents can be quantitatively determined from powdered concrete samples. The reliability of this method has been validated through Round-Robin (multi-laboratory) testing, which supports the use of acid-soluble analysis for measuring total chloride [19] and water-soluble analysis for free chloride [20]. Loser et al. [21] confirmed the applicability of this methodology for comparing chloride binding capacity across various binder systems. Similar analytical techniques have also been adopted in studies investigating chloride binding under marine exposure conditions [22].

4.3.2 Chloride binding isotherms

Chloride binding isotherms are widely employed to characterize the relationship between free chloride concentration and the amount of chloride bound within the cementitious matrix at a given temperature. These isotherms provide valuable insight into the binding behavior of concrete, which varies depending on the composition of the cementitious system [15] and significantly influences the rate of chloride ingress. As proposed by [23], chloride binding capacity can be quantified as the derivative ∂Cb/∂Cf, representing the change in bound chloride with respect to free chloride concentration. Experimental data are typically fitted to empirical or semi-empirical models, including the linear, Langmuir, and Freundlich isotherms, each offering different assumptions and mechanisms for describing the interaction between chlorides and hydration products. These models help quantify binding capacity and support a better understanding of chloride transport resistance in diverse binder systems. These three binding isotherms equations are shown hereafter:

Linear isotherm:

$$C_b = kC_f \, , \frac{\partial C_b}{\partial C_f} = k \tag{1}$$

Freundlich isotherm:

$$C_b = \alpha {C_f}^{\beta} \, , \, \frac{\partial C_b}{\partial Cf} = \alpha\beta {C_f}^{\beta-1} \tag{2}$$

Langmuir isotherm:

$$C_b = \frac{\alpha C_f}{1+\beta C_f} \ , \ \frac{\partial C_b}{\partial C_f} = \frac{\alpha}{(1+\beta C_f)^2} \tag{3}$$

In the above, Cb is the bound chloride content, Cf is the free chloride content, and α, β, and k are fitting parameters which have no physical meanings.

Despite their widespread use, the application of different chloride binding isotherms in concrete research remains not fully understood. As discussed in [15], the linear isotherm offers a simplified approach to modeling chloride binding in cementitious materials. While it provides a convenient and intuitive approximation, it tends to underestimate bound chloride at low free chloride concentrations and overestimate it at higher concentrations. Nevertheless, a linear relationship between free and bound chlorides has been observed in long-term field exposure studies, including marine environments over a 7-year period [24].

In contrast, the Freundlich and Langmuir isotherms are more widely adopted for modeling chloride binding due to their ability to capture nonlinear behavior. According to Tang and Nilsson [14], the Freundlich model is more appropriate when the external chloride concentration exceeds 0.01 mol/L, whereas the Langmuir model offers better accuracy at concentrations below 0.05 mol/L in cement paste and mortar systems. Laboratory studies on concrete specimens, however, have demonstrated that both models remain applicable. For example, Li and Jiang [11] reported high correlation coefficients for both isotherms under a 0.6 mol/L chloride exposure over a four-month bulk diffusion test. Furthermore, a review by Song et al. [25] concluded that linear, Freundlich, and Langmuir models have all been successfully applied to chloride binding in concrete. The use of modified fitting parameters across studies reflects the complexity of chloride binding behavior and suggests that a universally applicable model has yet to be established, especially for evaluations based on concrete specimens.

4.3.3 The influence of cementitious materials on chloride binding

4.3.3.1 Limestone filler

The partial replacement of clinker with limestone supports both economic and environmental sustainability objectives, while also exerting a multifaceted influence on chloride binding behavior in cementitious systems. From a physical standpoint, finely ground limestone particles act as nucleation sites, promoting the early formation of hydration products, particularly C-A-S-H gels [11]. This nucleation effect accelerates early-age hydration and contributes positively to chloride binding, especially at lower limestone replacement levels (e.g., around 10%). Chemically, limestone can react with tricalcium aluminate (C_3A) to form carboaluminate phases. The primary products of this reaction, monocarboaluminate (Mc) and hemicarboaluminate (Hc), have been shown to chemically bind chloride ions [26]. In a systematic study of chloride binding capacity, Bharadwaj et al. [6] reported that PLC retains effective chloride binding up to a 15% limestone replacement. Field evidence from the Portland Cement Association (PCA) [8] similarly confirmed that PLC with approximately 15% limestone did not negatively impact chloride ingress, as verified by 35-day chloride bulk diffusion tests conducted in accordance with ASTM C1556-22 [27].

However, higher levels of limestone replacement (e.g., >15%) may lead to detrimental effects, primarily due to the dilution effect [26]. At these levels, the reduction in clinker content limits the overall formation of hydration products—an effect that cannot be fully compensated by the nucleation benefit of limestone [28]. This results in reduced portlandite production, lowering the pH of the pore solution, which in turn facilitates the leaching of previously bound chlorides [11]. Moreover, as widely documented, AFm phases are the dominant hydrates responsible for chemical chloride binding [10,11]. The presence of excess limestone, however, stabilizes ettringite (AFt) and delays its transformation into AFm phases, thereby further reducing the system's chloride binding capacity at elevated limestone contents [29]. In summary, the chloride binding capacity of PLC concrete, particularly when the limestone replacement level exceeds current standard limits, remains not fully understood.

4.3.3.2 Fly ash

It is widely recognized that the influence of SCMs on chloride binding capacity, particularly through the formation of Cl-AFm phases, is strongly dependent on the aluminum oxide (Al_2O_3) content of the binder system [24,30,31]. Numerous studies have shown that the incorporation of fly ash enhances chloride binding, largely due to its relatively high Al_2O_3 content, often exceeding 15%. However, findings from Loser et al. [21], based on thermodynamic modeling, indicate that chloride binding is not solely governed by total Al_2O_3 content but also by the reactivity of the SCM. Their analysis revealed that only a small fraction, approximately 5%, of the Al_2O_3 in fly ash actively contributes to chloride binding reactions. As a result, when chloride binding is expressed as a function of total chloride input, mixtures containing fly ash may demonstrate lower overall bound chloride contents compared to those made with pure PC, despite having a higher total alumina content. However, under the incorporation of fly ash with limestone filler, the impact on chloride binding becomes more complex. On the one hand, the high Al_2O_3 content introduced by fly ash can enhance chemical chloride binding by promoting the formation of Cl-AFm phases. On the other hand, the synergistic effect between fly ash and limestone filler has been shown to stabilize AFt and delay its transformation into AFm phases [32], thereby introducing uncertainty in the overall enhancement of chloride binding.

4.3.3.3 Slag

Ground granulated blast-furnace slag (GGBFS) is another aluminum-rich supplementary cementitious material, typically containing 10–20% Al_2O_3 [33]. Like fly ash, numerous studies have demonstrated that slag incorporation enhances chloride binding capacity, primarily due to its alumina content [34,35]. The reactivity of slag can be preliminarily assessed using the basicity index, defined as the CaO/SiO_2 ratio; higher basicity values are generally associated with increased reactivity and, consequently, a greater potential for chloride binding [35]. However, not all slag types contribute equally. Slags with elevated sulfide or sulfur contents, such as sulfide-rich slags,

may hinder the formation of AFm phases, thereby reducing the overall chloride binding capacity [13].

In addition to total Al_2O_3 content, the Al_2O_3/SO_3 ratio is also a critical parameter influencing chloride binding behavior. Lower SO_3 content favors the preferential formation of AFm phases over AFt, thereby facilitating the formation of Friedel's salt and improving the immobilization of chloride ions [21]. These findings highlight the need to consider chemical composition when evaluating the effectiveness of SCMs in enhancing chloride resistance.

4.4 Scope of the work

Existing literature has focused on chloride binding in PC and SCMs, but chloride binding in low-carbon cementitious materials remains unexplored. Nowadays, the interground limestone replacement by clinker in PLC increased to 15% in Canada, followed by CSA A3000-23 [7] and some research results indicated that PLC with 15% replacement would not harm the chloride binding capacity. However, the further ambition of the low-carbon footprint raises concerns about chloride binding above the current standard limitation of limestone replacement level. This study aims to compare chloride binding in PLC concrete incorporating higher limestone replacement levels with or without SCMs by bulk diffusion test to simulate the non-steady state diffusion condition.

4.5 Materials and methods

4.5.1 Raw materials

The experimental variables included three levels of limestone replacement in PLC: one within the current CSA A3000 allowable limit of 15% (denoted as A), and two exceeding this threshold (H1 and H2), both containing over 20% interground limestone, with H2 having a slightly higher replacement level than H1. In addition, two types of supplementary cementitious materials (SCMs) were incorporated in selected mixtures: Type-F fly ash and slag. Natural sands with a maximum

size of 4.75 mm and limestone with sizes from 4.75 to 19mm were used in this study. Figure 4.1 shows the cumulative particle size distribution of the distinct cementitious material. Table 4.1 illustrates the chemical composition of the various cementitious materials.

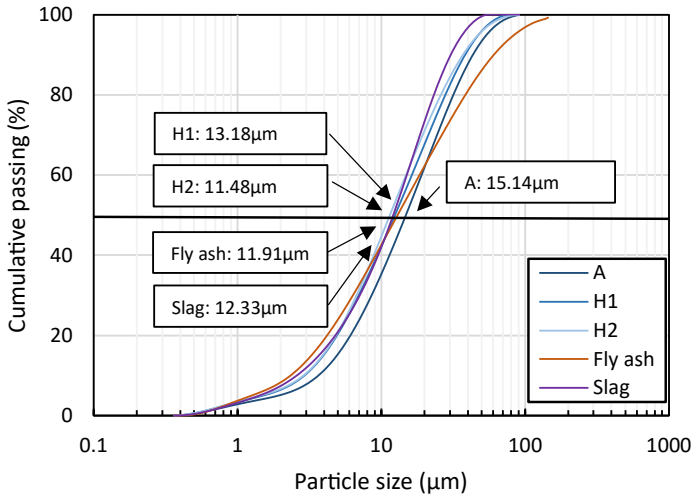

Figure 4.1. Particle size distribution of each cementitious material.

Table 4.1 Chemical composition & clinker phases of each cementitious material.

Mass (%)	**A**	**H1**	**H2**	**Slag**	**Fly ash**
CaO	62.19	60.83	60.87	41.45	14.22
SiO_2	18.71	17.71	17.20	36.52	49.27
Al_2O_3	4.51	4.27	4.09	10.54	16.24
Fe_2O_3	2.78	2.60	2.55	0.46	6.15
MgO	2.19	2.11	2.05	7.85	4.13
SO_3	2.95	4.62	4.42	0.24	0.68
K_2O	1.04	0.96	1.00	0.52	1.54
Na_2O	0.29	0.26	0.23	0.33	3.88
TiO_2	0.19	0.19	0.17	0.44	0.77
P_2O_5	0.13	0.13	0.12	0.00	0.40
MnO	0.06	0.05	0.06	0.29	0.06
LOI	6.23	9.217	10.05	1.36	1.29
C_3S	42.52	33.49	37.72	-	-
C_2S	17.79	20.74	16.31	-	-
C_3A	7.79	7.16	6.88	-	-
C_4AF	8.12	7.53	7.57	-	-
$CaCO_3$	13.34	21.39	22.47	-	-

As shown in Table 4.1, the chemical compositions of the three types of PLC cement, as determined by XRF analysis, reveal some unexpected trends. Notably, although cement H1 and H2 both contain high levels of interground limestone, with H2 exhibiting a slightly higher $CaCO_3$ content than H1 (i.e., 22.47 and 21.39, respectively), the measured CaO and K_2O contents in H2 are also slightly higher than those in H1. This is counterintuitive, as increased limestone replacement is expected to reduce the overall CaO content, given the lower reactivity of limestone compared to clinker. Additionally, SO_3 content, which primarily originates from gypsum rather than clinker phases, should remain relatively consistent across these cements, since limestone only partially replaces clinker. However, a significant variation in SO_3 levels is observed, further suggesting inconsistencies in the manufacturing process.

4.5.2 Mix proportions

A water-to-powder ratio (W/P) of 0.4 in accordance with the class C-1 exposure condition in CSA A23.1 [7] was selected for this research, and the concrete mix types were proportioned via the ACI method. High-range (HR) and mid-range (MR) water-reducing admixtures were added by mass of total powder in the mix to achieve ideal workability, and air-entrainment was added to the mix to provide 5-8% of air in accordance with the C-1 exposure condition requirement for preventing freezing and thawing cycles.

The detailed mix proportions are shown in Table 4.2. Fly ash and slag were marked as “F” and “S”, and each number followed by the abbreviation represents the replacement level of that specific cementitious material. For instance, “AF20” represents cement A + 20% fly ash blended in this powder system.

Table 4.2 Mix proportions.

Mixtures	W/P	Cement (kg/m^3)	SCMs* (kg/m^3)	Fine aggregate (kg/m^3)	Coarse aggregate (kg/m^3)	HR (kg/m^3)	MR (kg/m^3)	Air content** (%)
A	0.4	326	-	866	1179	3.26	3.26	5.7
H1	0.4	326	-	866	1179	3.26	3.26	5.5
H2	0.4	326	-	866	1179	3.26	3.26	5.9
AF20	0.4	261	65	866	1179	2.28	2.28	6.3
AF40	0.4	196	130	866	1179	2.28	2.28	6.6
H1F20	0.4	261	65	866	1179	2.28	2.28	7.1
H1F40	0.4	196	130	866	1179	2.28	2.28	6.8
H2F20	0.4	261	65	866	1179	2.28	2.28	7.1
H2F40	0.4	196	130	866	1179	2.28	2.28	6.2
AS20	0.4	261	65	866	1179	2.61	2.61	7.4
AS40	0.4	196	130	866	1179	2.61	2.61	6.8
H1S20	0.4	261	65	866	1179	2.61	2.61	7.5
H1S40	0.4	196	130	866	1179	2.61	2.61	6.8
H2S20	0.4	261	65	866	1179	2.61	2.61	6.1
H2S40	0.4	196	130	866	1179	2.61	2.61	6.8

*SCMs indicate fly ash or slag in accordance with the different mixture names.
**All the mixtures were air-entrained by adding air-entrainer followed by C-1 exposure; the air content of fresh state ranges from 5-8%.

4.5.3 Samples fabrication and curing process

Three test samples (100 mm in diameter, 200 mm in length) per family were cast and stored at 21 ± 1°C with over 90% relative humidity (RH) for 24 hours. After demolding, all the samples were cured in saturated calcium hydroxide water for 56 days to reduce the influence of hydration on the test outcomes. After curing, all the samples were prepared and tested in chloride bulk diffusion test.

4.5.4 Methods to measure bound chloride

The chloride bulk diffusion test was conducted in accordance with ASTM C1556-22 [27], which is widely used for evaluating chloride binding and resistance in concrete. Following a 56-day curing period, all concrete specimens were cut into cylinders measuring 100 mm in diameter and 75 mm in length. To ensure unidirectional chloride diffusion, the cylindrical sides and bottom surfaces

were sealed with epoxy resin, leaving only the top surface exposed. After allowing the epoxy to cure for 24 hours, specimens were submerged in a saturated calcium hydroxide solution for at least 24 additional hours to establish chemical equilibrium. Mass stability was then verified by confirming that the mass variation remained within ±0.1%. Once this condition was met, all specimens were immersed in a 165 g/L sodium chloride (NaCl) solution to begin the diffusion test. The solution was replaced monthly to maintain a stable external chloride concentration. After 90 days of exposure, the specimens were removed and prepared for chloride profiling. Chloride profiles were obtained by sequentially grinding the exposed surface in depth increments of 1–3 mm. The collected powders were oven-dried at 105 °C to a constant mass and then sieved through a 600 µm mesh to obtain homogeneous samples. Total and free chloride contents were determined by automatic potentiometric titration, following ASTM C1152-20 [36] for acid-soluble chlorides and ASTM C1218-20 [17] for water-soluble chlorides. A schematic of the chloride determination procedure is shown in Figure 4.2.

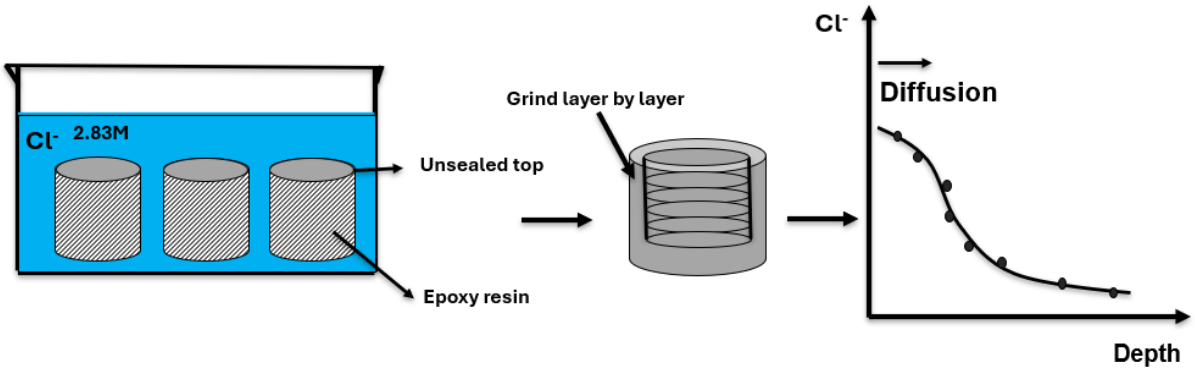

Figure 4.2. Schematic of chloride content determination process.

4.6 Results

The free and total chloride profiles with and without the addition of SCMs after 90-day NaCl solution immersion are given in Figure 4.3. Every chloride content point is determined by three samples of each mixture through automatic potentiometric titration of 5 g dry concrete powder.

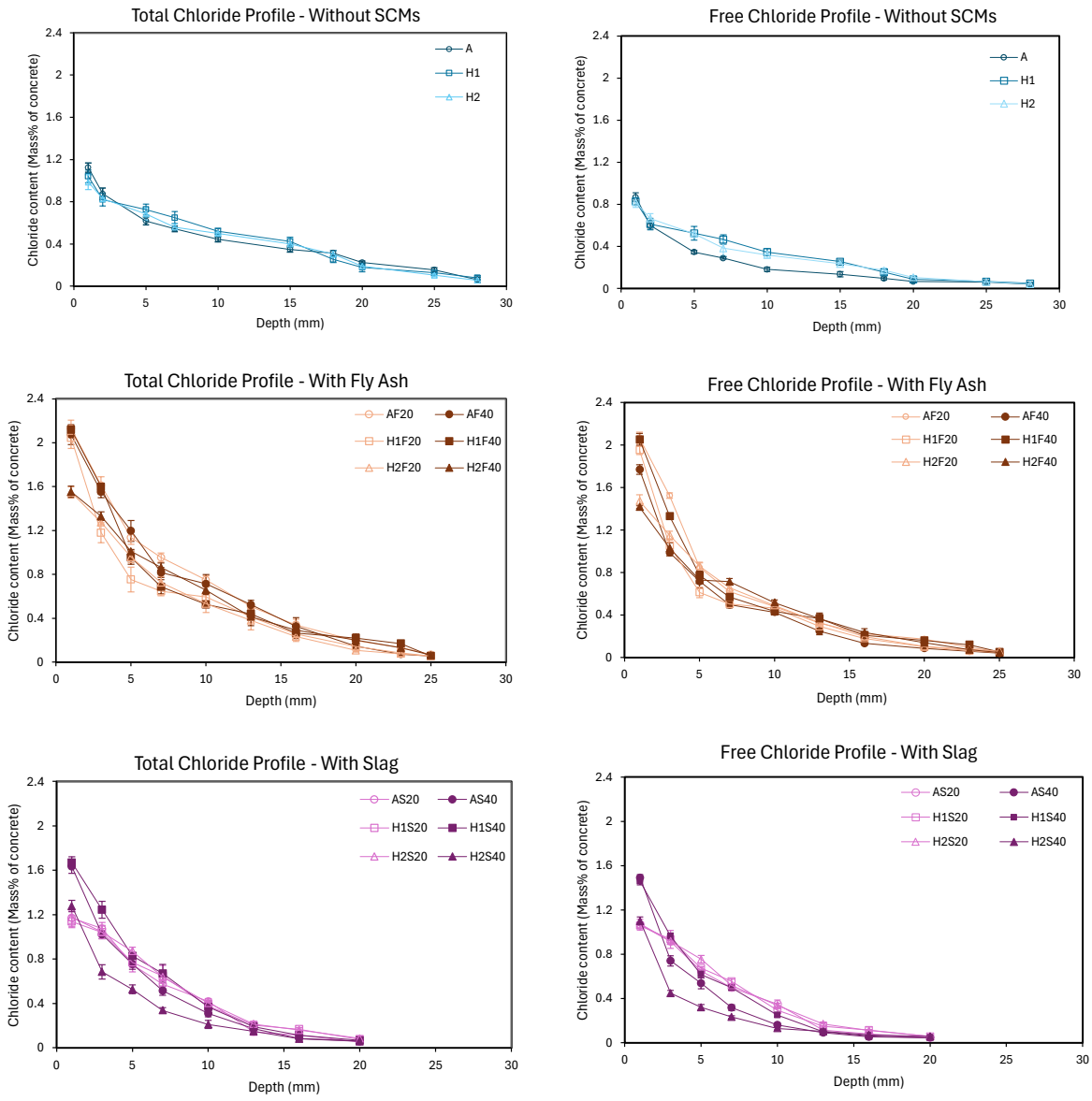

Figure 4.3. Total and free chloride profiles.

All mixtures exhibited a decreasing trend in chloride content with increasing depth from the exposed surface, consistent with typical chloride diffusion behavior in concrete. For the pure PLC mixtures (A, H1, and H2), the surface chloride concentrations were relatively similar, all remaining below 1.15% by dry mass. Among these, mixture A showed a steeper decline in total chloride content within the first 18 mm, indicating a potentially higher chloride binding capacity. This observation is further corroborated by the free chloride profiles, in which mixture A exhibited a more pronounced reduction in chloride concentration with depth compared to H1 and H2.

With the incorporation of fly ash, mixtures AF20, AF40, H1F20, and H2F40 exhibited comparable surface chloride concentrations, ranging from 2.04% to 2.14%. However, mixtures H2F20 and H2F40 demonstrated lower surface concentrations (between 1.49% and 1.61%), suggesting a potential synergistic effect between fly ash and higher limestone content. All fly ash–blended mixtures exhibited higher total chloride contents compared to their respective pure PLC counterparts, likely due to the increased Al_2O_3 content from fly ash, which promotes the formation of chloride binding AFm phases. The free chloride profiles for all six fly ash containing mixtures were more uniform, with background chloride levels reached at depths of approximately 23–25 mm. Among these, H1-based mixtures exhibited the highest free chloride concentrations near the surface, followed by A and H2-based systems. This trend may be attributed to the leaching of Friedel's salt, leading to elevated concentrations of free chloride in the superficial zone.

For slag containing mixtures, surface chloride concentrations were higher than those in pure PLC mixtures, but lower than those in fly ash blends with equivalent limestone replacement levels. This trend is consistent with the intermediate Al_2O_3 content of slag relative to PLC and fly ash. All slag containing mixtures reached background chloride levels at a shallower depth of approximately 20 mm, compared to both PLC and fly ash groups, which may be attributed to the ability of slag to refine pore structure and enhance resistance to chloride ingress. At 20% slag replacement, differences among mixtures A, H1, and H2 were marginal. However, increasing the slag content to 40% amplified these differences, highlighting the distinct influences of SCM content on chloride binding in PLC systems.

4.7 Discussion

4.7.1 Chloride binding with pure PLC mixtures

The bound chloride content of each mixture is determined by the differences between total and free chloride content. With the PLC mixtures (i.e., A, H1, and H2), the linear, Freundlich, and Langmuir isotherms are applied in this study to evaluate the chloride binding capacity, followed by Eq (1) -

Eq (3). The details are shown in Figure 4.4, and the fitting parameters and correlation coefficient (R^2) of each isotherm are depicted in Table 4.3.

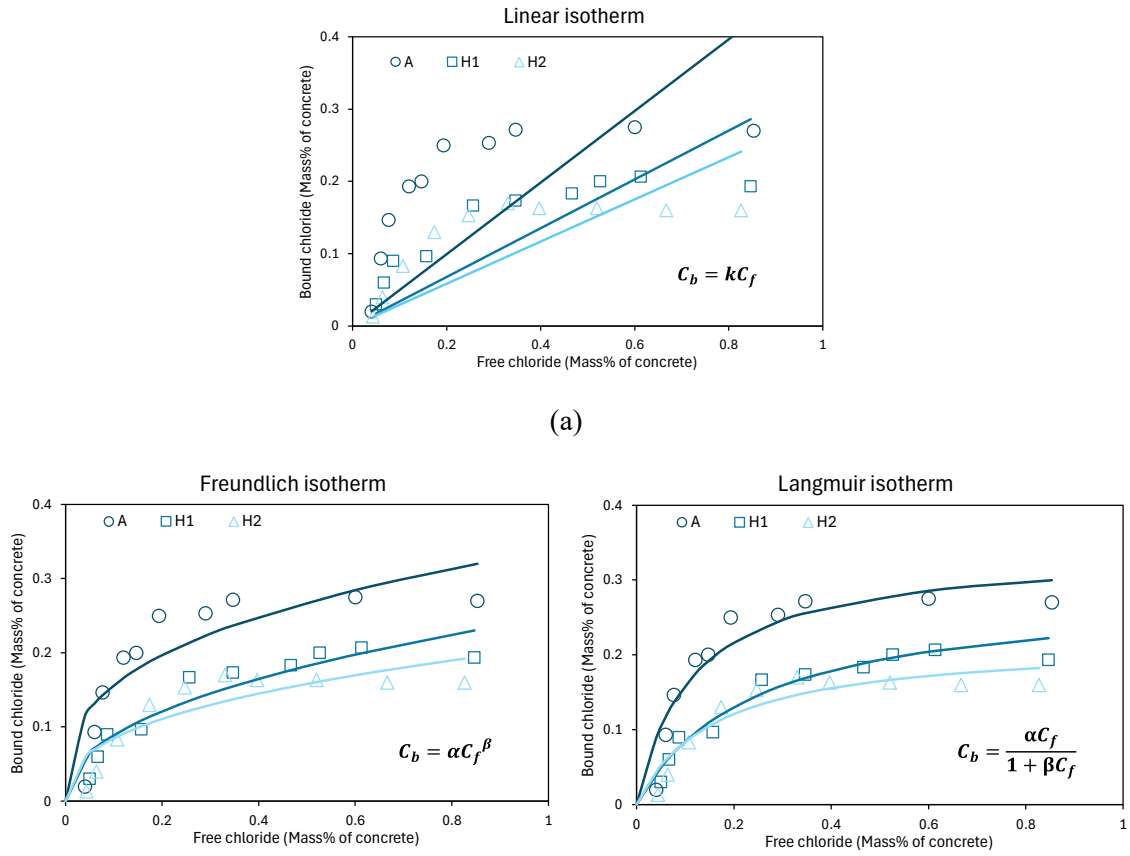

Figure 4.4 Different chloride binding isotherms in PLC without SCMs.

Table 4.3 Fitting parameters of each isotherm.

Mixtures	Linear isotherm		Freundlich isotherm			Langmuir isotherm		
	k	R^2	α	β	R^2	α	β	R^2
A	0.495	0.738	0.338	0.335	0.711	2.974	8.746	0.875
H1	0.338	0.887	0.248	0.445	0.877	1.199	4.208	0.948
H2	0.292	0.826	0.207	0.388	0.733	1.359	6.233	0.876

As shown in Fig 4.4, the highest bound chloride content was observed in mixture A, reaching 0.28%, followed by H1 and H2, with average values of 0.20% and 0.17%, respectively. When fitting the data using the linear isotherm, it was found that the model tends to underestimate bound

chloride content at low free chloride concentrations (i.e., below 0.4%) and overestimate it at higher concentrations. This phenomenon is consistent with findings reported in [13], which also highlight the limitations of the linear isotherm for capturing non-linear chloride binding behavior.

Among the three models evaluated, linear, Freundlich, and Langmuir isotherms, the Langmuir isotherm demonstrated the best fit for PLC mixtures in this study. This contrasts with the observations of Li and Jiang [11], who reported that both Freundlich and Langmuir models exhibited high R^2 values in describing the relationship between bound and free chloride in limestone filler blended cement concretes. The divergence in results may be attributed to differences in exposure conditions. In their study, the external chloride concentration was 35 g/L, simulating marine exposure. In contrast, the present study used a 165 g/L NaCl solution, following ASTM C1556-22 [27]. The high external chloride concentration, coupled with the absence of PH buffering, may accelerate portlandite leaching near the surface, leading to the dissolution and outward migration of previously bound chloride ions, as previously discussed in [21] and confirmed in [12]. This leaching effect appears to be more pronounced with the incorporation of SCMs, which influence pore solution chemistry and buffering capacity. A more detailed discussion of this phenomenon is presented in section 4.7.3.

Following the observation that the Langmuir isotherm exhibited the highest R^2 values among the three isotherm models applied to the PLC mixtures, the corresponding chloride binding capacity was further analyzed. Based on the definition of chloride binding capacity as the derivative $\partial Cb/\partial Cf$ [23], its variation as a function of free chloride concentration is illustrated in Fig 4.5. The analysis was conducted using the fitting parameters α and β derived from the Langmuir model, as presented in Table 4.3.

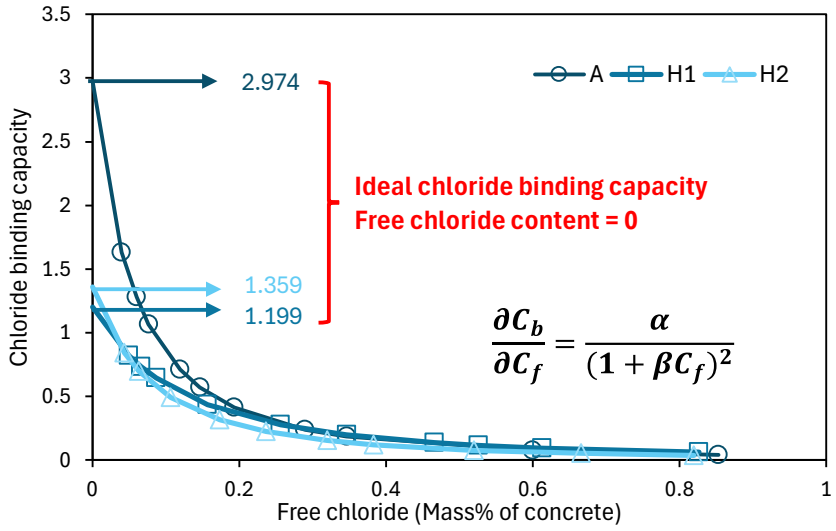

Figure 4.5. Ideal chloride binding capacity with PLC mixtures.

As illustrated in Fig 4.5, the chloride binding capacity of all three PLC mixtures decreases with increasing free chloride concentration. Mixture A consistently exhibits a higher binding curve compared to H1 and H2, although the curves begin to converge as the free chloride content increases. To facilitate comparison across mixtures, the concept of "ideal" chloride binding capacity is introduced, defined at the point where free chloride content is zero, assuming that all chloride ions are bound and retained within the matrix over time. This theoretical condition simplifies the evaluation of the maximum chloride binding potential of PLC systems with varying limestone replacement levels. Under this assumption, mixture A demonstrates the highest ideal binding capacity at 2.974, followed by H2 and H1, with values of 1.359 and 1.199, respectively. These differences suggest a reduction in chloride binding efficiency with increased limestone content. However, to validate whether these observed differences are statistically significant, a statistical analysis is required to assess the variability among the three mixtures and confirm the influence of limestone content on chloride binding performance.

To confirm the statistical significance of the differences in chloride binding capacities among the PLC mixtures, a one-way analysis of variance (ANOVA) was performed at a 95% confidence level. This analysis serves specifically to evaluate the influence of different cementitious material

compositions on chloride binding, rather than to validate the binding model itself. A similar approach of comparing the maximum bound chloride content among mixtures has also been adopted in previous studies, such as [21]. The detailed statistical results of the ANOVA are presented in Table 4.4.

Table 4.4. Statistical analysis of PLC.

Test mixtures	**F**	**F_{crit}**	**P**	**Significant**
Pure PLC	23.85	5.14	0.001	✓
PLC + Fly ash	59.92	3.11	4.55E-08	✓
PLC + Slag	12.52	3.11	0.0002	✓

Table 4.4 presents the statistical significance of the differences in bound chloride content among the PLC mixtures. To further evaluate whether the limestone replacement level has a statistically significant effect, a Tukey's Honestly Significant Difference (HSD) post hoc test was performed following the ANOVA. This test allows for pairwise comparisons between mixtures to identify which specific groups exhibit meaningful differences. According to the analysis, any comparison whose confidence interval crosses the reference line at zero is considered to show no statistically significant difference between the two mixtures. Conversely, if the interval does not intersect zero, the difference is regarded as statistically significant. The results of the Tukey HSD analysis are illustrated in Fig 4.6.

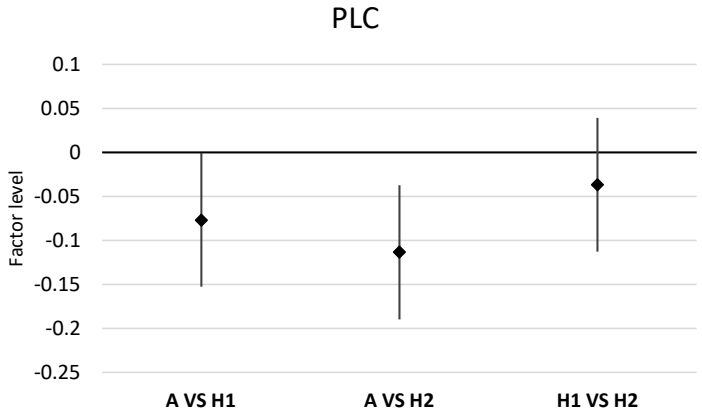

Figure 4.6. Tukey test of pure PLC mixtures.

As confirmed by the Tukey HSD test, mixture A exhibits a statistically significant difference in bound chloride content compared to both H1 and H2. In contrast, no significant difference was observed between H1 and H2. This trend is consistent with the results for ideal chloride binding capacity, where mixture A demonstrated a markedly higher value (2.974) compared to H1 (1.199) and H2 (1.359).

4.7.2 Al_2O_3/SO_3 ratio on pure PLC's chloride binding capacity

Based on the outcomes of the statistical analysis, the ideal chloride binding capacity values are found to be a reliable metric for comparing chloride binding performance among pure PLC mixtures. While it is widely accepted that a higher Al_2O_3 content in cementitious materials enhances chemical chloride binding by promoting the formation of aluminate phases, this trend is not fully reflected in the present study. As shown in Table 4.1, the Al_2O_3 content differences among mixtures A, H1, and H2 are minimal, within approximately 0.5%, and their decreasing trend from A to H2 does not correspond proportionally with the decline in chloride binding capacity observed in Section 6.1. As highlighted by Loser et al. [21], the Al_2O_3/SO_3 ratio serves as a more meaningful indicator of chemical chloride binding capacity, since SO_3 promotes the stabilization of AFt phases, thereby delaying the transformation to chloride-binding AFm phases [13]. Figure 8 presents the Al_2O_3/SO_3 ratio alongside the ideal chloride binding capacity for each PLC mixture, illustrating the correlation between these two factors and reinforcing the importance of sulfate–alumina balance in optimizing chloride binding performance.

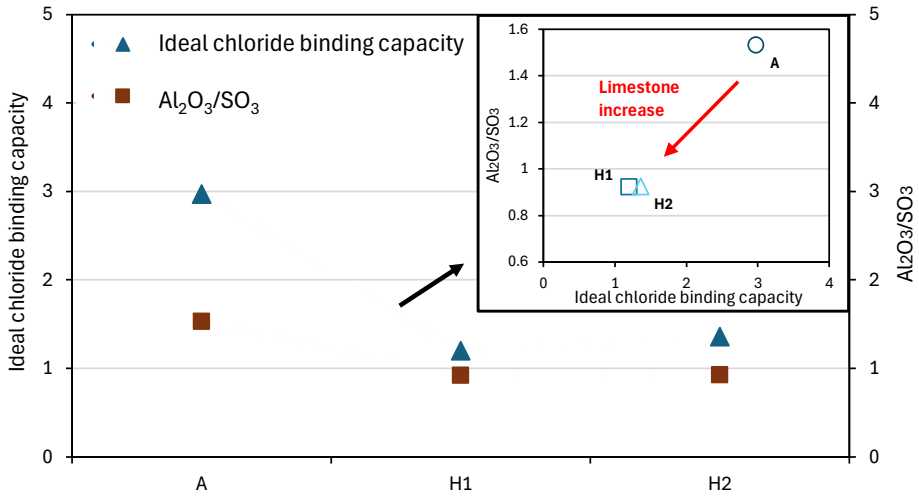

Figure 4.7. The relationship between ideal chloride binding capacity and Al_2O_3/SO_3.

From Figure 4.7, the Al_2O_3/SO_3 ratio and ideal chloride binding capacity display a similar trend. Where A shows the highest Al_2O_3/SO_3 ratio of 1.532, then followed by H1 and H2, which are 0.923 and 0.925, respectively. It could prove that Al_2O_3/SO_3 is a more suitable indicator of chloride binding capacity in pure PLC mixtures than singular Al_2O_3 content, and only Al_2O_3 content seems oversimplified to quantify the chloride binding capacity in pure PLC concrete. However, this raises another interesting point of discussion. From A to H2, the observed differences in chloride binding capacity appear to be primarily influenced by variations in SO_3 content, despite relatively minor differences in their overall chemical compositions. Notably, the original intent behind increasing interground limestone content in PLC was not to introduce significant changes in SO_3 levels. From a cement manufacturing perspective, most of the SO_3 originates from gypsum rather than from clinker phases. Therefore, increasing limestone replacement at the expense of clinker should not inherently lead to substantial changes in SO_3 content. In the context of this study, the notable variation in SO_3 is most likely a result of industry-specific manufacturing processes rather than the limestone content itself. This distinction is important, as it suggests that higher limestone replacement levels in PLC may not necessarily compromise chloride binding performance. If the cement manufacturing process can be reasonably controlled, it opens up greater potential for the future application of high interground limestone PLCs.

4.7.3 Chloride binding with binary blended PLC

Figure 4.8 presents the relationship between bound and free chloride content in binary blended PLC mixtures. It is evident that the incorporation of SCMs results in a marked decrease in bound chloride content near the exposure surface. As discussed in Section 6.1, this behavior is attributed to leaching caused by the high external chloride concentration of the exposure solution. A similar leaching effect has also been reported by Loser et al. [21]. Under such conditions, it is not appropriate to apply chloride binding isotherms for calculating ideal chloride binding capacity, as the results are distorted by the leaching of previously bound chlorides. Consequently, in the following sections, bound chloride content will be used, following the methodology of [21], to compare the chloride binding performance among mixtures.

Mixtures with 40% fly ash exhibit significantly higher chloride binding than those with 20% fly ash, supporting the notion that increased fly ash content enhances chloride binding by reducing free chloride concentrations. This improvement is likely due to the high Al_2O_3 content in fly ash, which promotes the transformation of AFt to AFm phases. Among all mixtures, AF40 shows the highest bound chloride content, approaching 0.6%, confirming the effectiveness of high-volume fly ash in enhancing chemical binding. It is also noteworthy that, at both fly ash replacement levels (20% and 40%), mixtures H1 and H2 exhibit similar levels of bound chloride, suggesting a limited influence of further increasing limestone content under fly ash blended conditions. A more detailed discussion of this trend will follow.

For slag blended mixtures, those with 20% slag replacement exhibit similar bound chloride contents. However, increasing the slag content to 40% results in comparable chloride binding with mixture A, with maximum values approaching 0.3%. When comparing the performance of fly ash and slag, the higher chloride binding capacity of fly ash is primarily attributed to its greater Al_2O_3 content compared to A, H1, and H2, as summarized in Table 4.1.

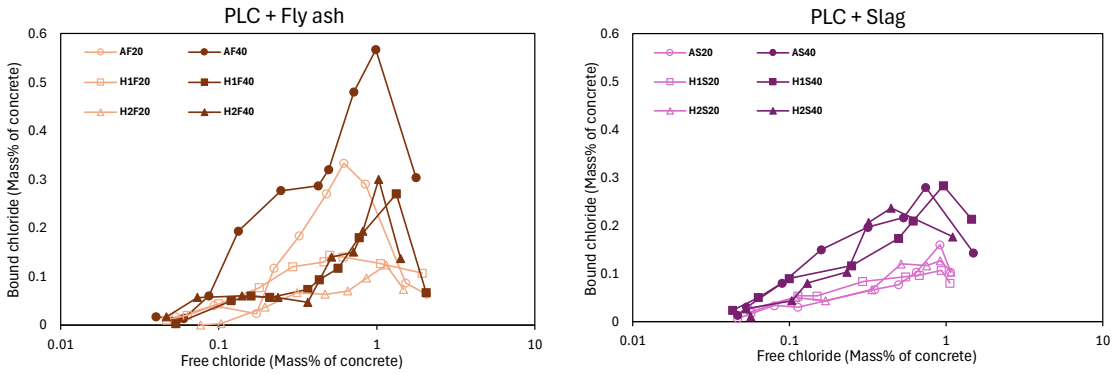

(a) (b)

Figure 4.8. The relationship between bound and free chloride in binary blended PLC: (a) PLC + Fly ash, and (b) PLC + Slag.

To more rigorously evaluate the effect of limestone content on chloride binding, a Tukey's post-hoc test was conducted to assess the statistical significance of differences among mixtures. This approach, consistent with the methodology described as aforementioned, provides a more reliable basis for comparison. The detailed results of this analysis are presented in Figure 4.9.

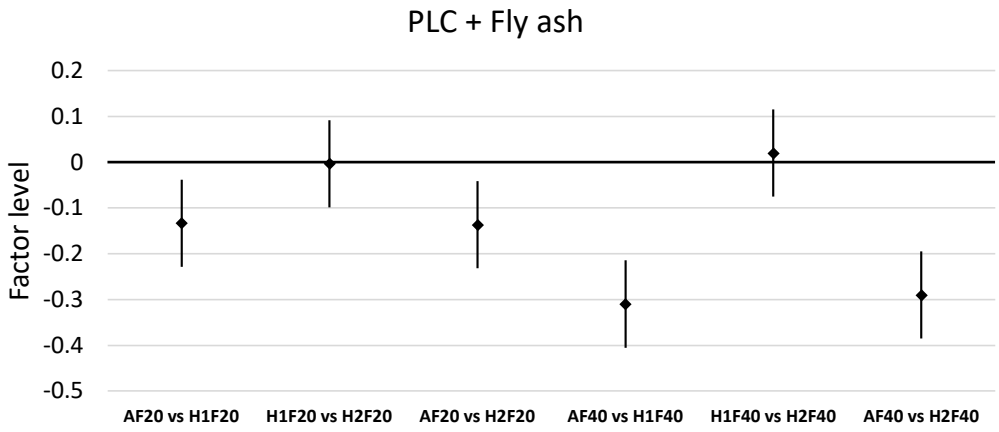

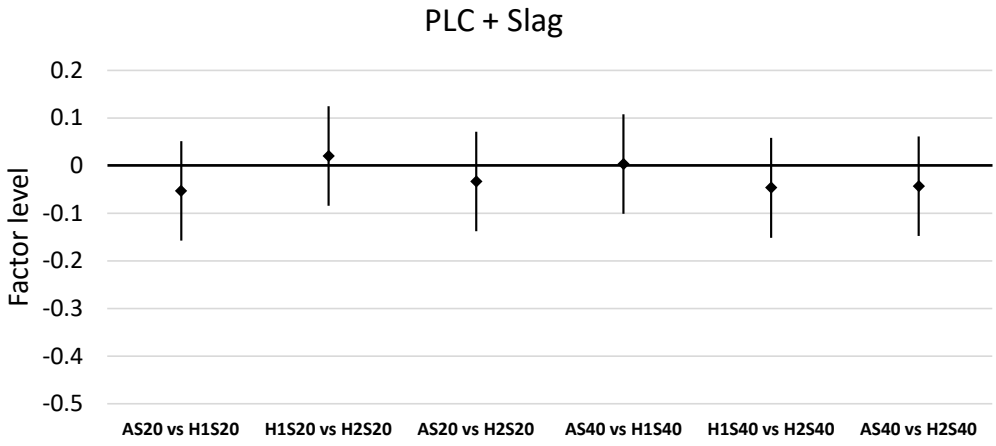

Figure 4.9. Tukey test of binary blended PLC mixtures.

Through Tukey's test, incorporated with fly ash replacement, the above limitation (H1 and H2) does not have a significant impact on chloride binding at both fly ash replacement levels (20% and 40%). One possible explanation lies in the nature of fly ash as a pozzolanic material, which contains only a small amount of CaO. Under such conditions, its reactivity is highly dependent on the availability of hydration products generated by the PLC matrix to trigger pozzolanic reactions. This may explain why the chloride binding trend observed in fly ash blended mixtures is similar to that of pure PLC mixtures. Therefore, when discussing chloride binding in PLC–fly ash systems, the role of fly ash during the 90-day diffusion test can be interpreted as acting similarly to an alumina-enriched PLC, due to its high Al_2O_3 content. However, as observed from the overall chloride resistance results in the previous section, the influence of fly ash on chloride binding is not clearly reflected in the short-term (i.e., 90-day) diffusion test. This suggests that the enhancement in chloride binding capacity attributed to fly ash may not immediately translate into improved resistance to chloride ingress within this limited time frame. Nonetheless, based on existing literature, chloride binding is recognized as a time-dependent process, and its contribution becomes more pronounced over extended exposure durations. Therefore, long-term testing is essential for a more accurate assessment of chloride binding performance in PLC–fly ash systems.

With the addition of slag, statistical analysis confirms that increasing the limestone replacement level from low limestone replacement level (i.e., A) to high limestone replacement (i.e., H1 and H2) does not result in a significant difference in bound chloride content. This indicates that the variation in chloride binding capacity is negligible within this range under slag-blended conditions. A likely explanation is that, in contrast to fly ash, slag contains a higher CaO content and is less dependent on pozzolanic reaction for the formation of C-A-S-H phases. As fly ash typically requires extended periods to contribute to secondary hydration, slag can more readily react and form hydration products independently. These results also indicate that, although SO_3 content plays a role in differentiating chloride binding capacity among pure PLC mixtures, such influence appears to be mitigated in systems incorporating slag. In these mixtures, slag exerts a dominant influence on chloride binding behavior, effectively reducing the variability introduced by sulfate-related effects and reinforcing its importance in chemical chloride binding.

It is also important to note that, contrary to expectations, even with 40% slag addition, the bound chloride content only reaches a level comparable to that of mixture A. In this study, the slag used is assumed to be relatively reactive, with a basicity ratio (CaO/SiO_2) of 1.13, as calculated from Table 4.1, a value greater than 1, which typically promotes the formation of additional C-A-S-H phases. However, as summarized by Lothenbach et al. [37], a substantial portion of the Al_2O_3 in slag tends to be incorporated into C-A-S-H, rather than forming AFm phases, thereby limiting the formation of Friedel's salt in the short term. This aligns with the findings by De Weerdt et al. [10], who noted that only 10–20% of C-A-S-H contributes to strong chloride binding via physical mechanisms. Therefore, despite the higher reactivity and greater Al_2O_3 content of slag compared to PLC, its ability to enhance chloride binding during the short 90-day bulk diffusion test remains limited. These findings also provide a strong explanation for the observations in the previous section: although the bound chloride content of 40% slag mixtures was similar to that of mixture A, the overall chloride resistance was markedly greater. This is attributed to the refinement of the

pore structure through increased C-A-S-H formation, which significantly reduces chloride ingress. However, the contribution of C-A-S-H to chloride binding remains limited, thereby explaining the consistency in trends observed between chloride resistance and chloride binding in the slag-incorporated mixtures (20% and 40%).

4.8 Conclusion

In this paper, the chloride binding of PLC with and without the addition of fly ash or slag is determined by the acid-soluble and water-soluble concrete powder after a 3-month bulk diffusion test. The main findings are shown hereafter:

- Among three chloride binding isotherms, Langmuir isotherm shows the highest correlation coefficient (R^2) in pure PLC mixtures under high concentration external solution with 0.4 W/P ratio, and ideal chloride binding capacity is a suitable indicator to be used in pure PLC mixtures in chloride binding for comparison reasons.
- It would be better to use the Al_2O_3/SO_3 than simple Al_2O_3 content to explain this phenomenon and the higher ratio results in a higher chloride binding. However, it would be premature to conclude that further increases in interground limestone content inherently lead to a reduction in chloride binding capacity. The observed differences are more likely attributed to variations in the cement manufacturing process, rather than the limestone replacement level itself, particularly due to imbalanced gypsum phases. This distinction emphasizes the critical role of controlled production parameters and optimized manufacturing practices in ensuring consistent performance. By addressing these factors, greater opportunities for the sustainable development of cement can be realized, allowing for higher limestone content without compromising key durability characteristics like chloride resistance.
- With the addition of SCMs, fly ash and slag show different chloride binding performances. Fly ash blended mixtures rely heavily on the chloride binding behavior of pure PLC

systems due to its pozzolanic nature, which depends on the availability of primary hydration products. In contrast, slag blended mixtures exhibit more independent behavior and are less influenced by variations in different unexpected chemical compositions in A, H1, and H2.

4.9 References

[1] M. T. De Grazia, H. Deda, and L. F.M. Sanchez, "The influence of the binder type & aggregate nature on the electrical resistivity of conventional concrete," J. Build. Eng., vol. 43, p. 102540, Nov. 2021, doi: 10.1016/j.jobe.2021.102540.

[2] K. L. Scrivener, V. M. John, and E. M. Gartner, "Eco-efficient cements: Potential economically viable solutions for a low-CO2 cement-based materials industry," Cem. Concr. Res., vol. 114, pp. 2–26, Dec. 2018, doi: 10.1016/j.cemconres.2018.03.015.

[3] "Cement and Concrete: The Environmental Impact," PSCI. Accessed: May 12, 2025. [Online]. Available: https://psci.princeton.edu/tips/2020/11/3/cement-and-concrete-the-environmental-impact

[4] M. T. de Grazia, L. F. M. Sanchez, R. C. O. Romano, and R. G. Pileggi, "Investigation of the use of continuous particle packing models (PPMs) on the fresh and hardened properties of low-cement concrete (LCC) systems," Constr. Build. Mater., vol. 195, pp. 524–536, Jan. 2019, doi: 10.1016/j.conbuildmat.2018.11.051.

[5] I. Government of Canada, "Net Zero Accelerator Initiative." Accessed: Sep. 02, 2024. Available: https://ised-isde.canada.ca/site/strategic-innovation-fund/en/net-zero-accelerator-initiative

[6] B. Lothenbach, K. Scrivener, and R. D. Hooton, "Supplementary cementitious materials," Cem. Concr. Res., vol. 41, no. 12, pp. 1244–1256, Dec. 2011, doi: 10.1016/j.cemconres.2010.12.001.

[7] CSA Group, Cementitious Materials Compendium, CSA A3000:23, Toronto, ON, Canada, 2023.

[8] K. Bharadwaj et al., "CALTRANS: Impact of the Use of Portland-Limestone Cement on Concrete Performance as Plain or Reinforced Material," Kiewit Center, Nov. 2021. doi: 10.5399/osu/1150.

[9] CSA A23.1:19-CSA%20A23.2:19/ Concrete materials and methods of concrete construction/Test Methods and Standard Practices for concrete.

[10] Portland Cement Association et al., "State-of-the-Art Report on Use of Limestone in Cements at Levels of up to 15%," Portland Cement Association, 2024. doi: 10.70909/pca.2024.SN3148.03.

[11] T. Dyer, Concrete Durability. Boca Raton, FL, USA: CRC Press, 2014.

[12] K. De Weerdt, W. Wilson, A. Machner, and F. Georget, “Chloride profiles – What do they tell us and how should they be used?,” Cem. Concr. Res., vol. 173, p. 107287, Nov. 2023, doi: 10.1016/j.cemconres.2023.107287.

[13] C. Li and L. Jiang, “The role of chloride binding mechanism in the interpretation of chloride profiles in concrete containing limestone powder,” J. Sustain. Cem.-Based Mater., vol. 12, no. 1, pp. 24–35, Jan. 2023, doi: 10.1080/21650373.2021.2010243.

[14] A. Machner, M. Bjørndal, A. Šajna, N. Mikanovic, and K. De Weerdt, “Impact of leaching on chloride ingress profiles in concrete,” Mater. Struct., vol. 55, no. 1, pp. 1–18, Jan. 2022, doi: 10.1617/s11527-021-01730-w.

[15] Q. Yuan, C. Shi, G. De Schutter, K. Audenaert, and D. Deng, “Chloride binding of cement-based materials subjected to external chloride environment – A review,” Constr. Build. Mater., vol. 23, no. 1, pp. 1–13, Jan. 2009, doi: 10.1016/j.conbuildmat.2008.02.004.

[16] T. Luping and L.-O. Nilsson, “Chloride binding capacity and binding isotherms of OPC pastes and mortars,” Cem. Concr. Res., vol. 23, no. 2, pp. 247–253, Mar. 1993, doi: 10.1016/0008-8846(93)90089-R.

[17] B. Martín-Pérez, H. Zibara, R. D. Hooton, and M. D. A. Thomas, “A study of the effect of chloride binding on service life predictions,” Cem. Concr. Res., vol. 30, no. 8, pp. 1215–1223, Aug. 2000, doi: 10.1016/S0008-8846(00)00339-2.

[18] Chloride penetration into concrete, State-of-the-Art. Transport processes, corrosion initiation, test methods and prediction models,” Available: https://www.researchgate.net/publication/264420368_HETEK_Chloride_penetration_into_concrete_State-of-the - Art_Transport_processes_corrosion_initiation_test_methods_and_prediction_models

[19] ASTM C1218/C1218M-20 Standard Test Method for Water-Soluble Chloride in Mortar and Concrete, ASTM International, 2020.

[20] RILEM TC 178-TMC, “RILEM TC 178-TMC: ’Testing and modelling chloride penetration in concrete’Analysis of water soluble chloride content in concrete,” Mater. Struct., vol. 35, no. 253, pp. 586–588, Sep. 2002, doi: 10.1617/13841.

[21] M. Castellote and C. Andrade, “Round-Robin test on chloride analysis in concrete—Part I: Analysis of total chloride content,” Mater. Struct., vol. 34, no. 9, pp. 532–549, Nov. 2001, doi: 10.1007/BF02482181.

[22] M. Castellote and C. Andrade, “Round-robin test on chloride analysis in concrete — Part II: Analysis of water soluble chloride content,” Mater. Struct., vol. 34, no. 10, pp. 589–596, Dec. 2001, doi: 10.1007/BF02482124.

[23] R. Loser, B. Lothenbach, A. Leemann, and M. Tuchschmid, “Chloride resistance of concrete and its binding capacity – Comparison between experimental results and thermodynamic modeling,” Cem. Concr. Compos., vol. 32, no. 1, pp. 34–42, Jan. 2010, doi: 10.1016/j.cemconcomp.2009.08.001.

[24] Y. Wang, C. Liu, Y. Tan, Y. Wang, and Q. Li, “Chloride binding capacity of green concrete mixed with fly ash or coal gangue in the marine environment,” Constr. Build. Mater., vol. 242, p. 118006, May 2020, doi: 10.1016/j.conbuildmat.2020.118006.

[25] L. O. Nilsson, M. Massat, and L. Tang, “Effect of Non-Linear Chloride Binding on the Prediction of Chloride Penetration Into Concrete Structures”, Accessed: Mar. 15, 2025. [Online]. Available: https://www.concrete.org/publications/internationalconcreteabstractsportal.aspx?m=details&id=4554

[26] T. Cheewaket, C. Jaturapitakkul, and W. Chalee, “Long term performance of chloride binding capacity in fly ash concrete in a marine environment,” Constr. Build. Mater., vol. 24, no. 8, pp. 1352–1357, Aug. 2010, doi: 10.1016/j.conbuildmat.2009.12.039.

[27] C. Song, C. Jiang, X.-L. Gu, Q. Zhang, and W.-P. Zhang, “Calibration analysis of chloride binding capacity for cement-based materials under various exposure conditions,” Constr. Build. Mater., vol. 314, p. 125588, Jan. 2022, doi: 10.1016/j.conbuildmat.2021.125588.

[28] S. Sui et al., “Quantification methods for chloride binding in Portland cement and limestone systems,” Cem. Concr. Res., vol. 125, p. 105864, Nov. 2019, doi: 10.1016/j.cemconres.2019.105864.

[29] ASTM C1556-22 Standard Test Method for Determining the Apparent Chloride Diffusion Coefficient of Cementitious Mixtures by Bulk Diffusion, ASTM International, 2022.

[30] A. C. Bergmann et al., “Influence of Interparticle Separation Distance on the Fresh and Hardened Behavior of Ecoefficient Cement Pastes,” J. Mater. Civ. Eng., vol. 35, no. 8, p. 04023252, Aug. 2023, doi: 10.1061/JMCEE7.MTENG-14988.

[31] G. Kakali, S. Tsivilis, E. Aggeli, and M. Bati, “Hydration products of C3A, C3S and Portland cement in the presence of CaCO3,” Cem. Concr. Res., vol. 30, no. 7, pp. 1073–1077, Jul. 2000, doi: 10.1016/S0008-8846(00)00292-1.

[32] Z. Yang et al., “Improving the chloride binding capacity of cement paste by adding nano-Al2O3: The cases of blended cement pastes,” Constr. Build. Mater., vol. 232, p. 117219, Jan. 2020, doi: 10.1016/j.conbuildmat.2019.117219.

[33] E. G. Moffatt and M. D. A. Thomas, “Performance of 25-year-old silica fume and fly ash lightweight concrete blocks in a harsh marine environment,” Cem. Concr. Res., vol. 113, pp. 65–73, Nov. 2018, doi: 10.1016/j.cemconres.2018.07.004.

[34] C. Yi et al., “Study on chloride binding capability of coal gangue based cementitious materials,” Constr. Build. Mater., vol. 167, pp. 649–656, Apr. 2018, doi: 10.1016/j.conbuildmat.2018.02.071.

[35] O. R. Ogirigbo and L. Black, “Chloride binding and diffusion in slag blends: Influence of slag composition and temperature,” Constr. Build. Mater., vol. 149, pp. 816–825, Sep. 2017, doi: 10.1016/j.conbuildmat.2017.05.184.

[36] J. O. Ukpata, P. A. M. Basheer, and L. Black, “Slag hydration and chloride binding in slag cements exposed to a combined chloride-sulphate solution,” Constr. Build. Mater., vol. 195, pp. 238–248, Jan. 2019, doi: 10.1016/j.conbuildmat.2018.11.055.

[37] ASTM C595/C595M-24 Standard Specification for Blended Hydraulic Cements, ASTM International, 2024.

[38] “BS EN 12390-11:2015 - TC | 31 Aug 2015 | BSI Knowledge.” Accessed: Mar. 12, 2025. Available: https://knowledge.bsigroup.com/products/testing-hardened-concrete-determination-of-the-chloride-resistance-of-concrete-unidirectional-diffusion

[39] ASTM C1152/C1152M-20 Standard Test Method for Acid-Soluble Chloride in Mortar and Concrete, ASTM International, 2020.

[40] M. Thomas and T. Bremner, “Performance of lightweight aggregate concrete containing slag after 25years in a harsh marine environment,” Cem. Concr. Res., vol. 42, no. 2, pp. 358–364, Feb. 2012, doi: 10.1016/j.cemconres.2011.10.009.

[41] Z. Yang, Y. Gao, S. Mu, H. Chang, W. Sun, and J. Jiang, “Improving the chloride binding capacity of cement paste by adding nano-Al2O3,” Constr. Build. Mater., vol. 195, pp. 415–422, Jan. 2019, doi: 10.1016/j.conbuildmat.2018.11.012.

[42] K. De Weerdt, K. O. Kjellsen, E. Sellevold, and H. Justnes, “Synergy between fly ash and limestone powder in ternary cements,” Cem. Concr. Compos., vol. 33, no. 1, pp. 30–38, Jan. 2011, doi: 10.1016/j.cemconcomp.2010.09.006.

[43] B. Lothenbach, K. Scrivener, and R. D. Hooton, “Supplementary cementitious materials,” Cem. Concr. Res., vol. 41, no. 12, pp. 1244–1256, Dec. 2011, doi: 10.1016/j.cemconres.2010.12.001.

Chapter 5

Conclusion and Future gaps

5.1 Conclusion

This study systematically investigated the chloride resistance and chloride binding behavior of Portland-limestone cement (PLC) concrete mixtures, incorporating varying levels of interground limestone and different types of supplementary cementitious materials (SCMs), including fly ash and slag. A combination of diffusion testing and acceleration tests was employed to assess durability performance and binding mechanisms.

- Key findings reveal that the water-to-clinker ratio is a more reliable indicator of chloride resistance than the water-to-powder (W/P) ratio, especially in systems with high limestone content (i.e., greater than 15%). Moreover, a strong correlation between bulk ER, surface ER, and the apparent diffusion coefficient (Da) confirms that pore structure refinement, achieved through SCM incorporation, plays a critical role in resisting chloride ingress. However, the rapid chloride permeability test (RCPT) proved insufficiently sensitive to distinguish between pure PLC mixtures, indicating the need for more optimization for low-resistivity systems.

- In terms of chloride binding, results show that the Langmuir isotherm provides the best fit for pure PLC mixtures among three isotherms. Moreover, the Al_2O_3/SO_3 ratio serves as a more meaningful indicator of chloride binding capacity than the Al_2O_3 content. Importantly, the observed reduction in chloride binding with increased limestone content is likely due to manufacturing inconsistencies, particularly in gypsum content, rather than the limestone replacement itself. This underscores the need for improved quality control in cement manufacturing to maintain durability performance at higher replacement levels.

- Finally, fly ash and slag exhibited distinct binding behaviors: fly ash performance closely followed trends in the pure PLC system, while slag blended mixtures demonstrated more independent behavior, less affected by variations in distinct PLC chemical composition. These insights contribute to the development of sustainable, durable PLC systems and support the feasibility of further increasing limestone content when paired with optimized mix designs and controlled manufacturing practices.

5.2 Future gaps

Future research recommendations regarding chloride resistance and its binding performance of PLC concrete are presented hereafter:

- In PLC systems, understanding the actual existing chloride ions is critical for evaluating durability. During bulk diffusion testing, simulating marine exposure conditions can help replicate actual chloride ingress processes and better assess performance under aggressive environments.
- Additionally, variations in pH play a significant role in influencing chloride resistance, particularly in terms of chloride binding capacity. Establishing test environments with different pH levels is therefore an essential aspect of research on low-carbon cementitious systems and their long-term durability against chloride ingress.
- To further support chloride binding evaluations, phase composition analyses, such as X-ray diffraction (XRD) and thermogravimetric analysis (TGA), can be employed to identify and quantify hydration products, such as AFm, C-A-S-H, and AFt phases, formed in various PLC systems. These analytical techniques provide insight that may account for differences in chloride binding behavior across different binder compositions.
- It is also important to note that while chloride binding is an influential factor in determining overall chloride resistance, its impact may be limited in short-term bulk diffusion tests. As

such, long-term performance testing is still necessary to fully understand the evolution of chloride binding and resistance mechanisms over time in PLC concretes.

Appendix A

Chloride determination

A.1 Total chloride titration

After collecting powdered samples from each depth increment, the material was passed through a 600 µm sieve to ensure uniform particle size. For the chloride content determination, approximately 5 g of the sieved powder was dissolved in 75 mL of deionized water, followed by the addition of 25 mL of 50% diluted nitric acid (1:1 ratio of water to acid) and 3 mL of 30% hydrogen peroxide. The solution was continuously stirred and heated on a hot plate. Once condensation appeared on the underside of the watch glass cover, indicating sufficient vaporization, the heating was stopped and the solution was filtered to remove solid residues. After cooling, the filtrate was transferred to the potentiometric titration setup for chloride determination using 0.1 N silver nitrate ($AgNO_3$). In cases where the chloride content was expected to be low (typically less than 0.15% by mass), the powder mass was increased to 10 g to improve titration accuracy. Using insufficient sample quantities in low-chloride scenarios may cause greater potential drift during titration, making end-point detection more difficult. The detailed procedure is illustrated hereafter.

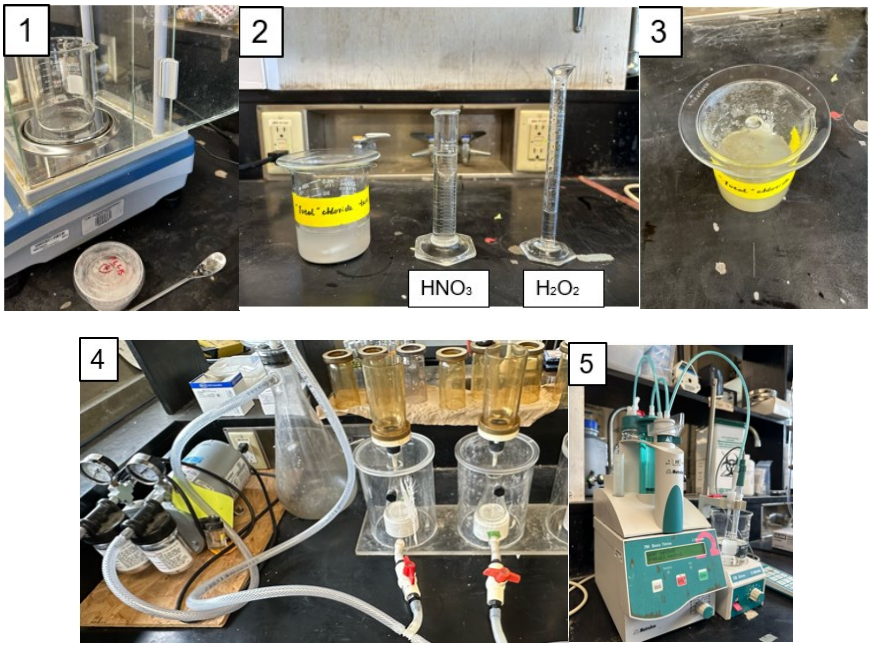

A.2 Free chloride titration

For the determination of water-soluble chloride content, the same powder samples used for total chloride titration were employed. Approximately 5 g of the sieved powder was dissolved in deionized water, with continuous stirring and gentle heating applied. Heating was maintained until the characteristic condensation appeared on the inner surface of the watch glass, indicating sufficient dissolution. The solution was then removed from the heat and allowed to cool to ambient temperature, after which it was stored for 24 hours to enable adequate precipitation. Following the resting period, the solution was filtered, and 3 mL of 50% diluted nitric acid along with 3 mL of 30% hydrogen peroxide was added to the filtrate. The mixture was then reheated and transferred to a 60 mL beaker for potentiometric titration using 0.1 N silver nitrate, following the same procedure used for total chloride determination. The reduced solution volume in this method reflects the typically lower chloride concentrations associated with the free (mobile) chloride fraction. The complete procedure is illustrated hereafter.